Inorg. Chem. **2006**, *45*, 695–709

A New Family of Ruthenium(II) Polypyridine Complexes Bearing 5-Aryltetrazolate Ligands as Systems for Electrochemiluminescent Devices

Stefano Stagni,[†] Antonio Palazzi,*[,†] Stefano Zacchini,[†] Barbara Ballarin,[†] Carlo Bruno,[‡] Massimo Marcaccio,*[,‡] Francesco Paolucci,[‡] Magda Monari,[‡] Maurizio Carano,[§] and Allen J. Bard*[,§]

Dipartimento di Chimica Fisica ed Inorganica, Università di Bologna, viale Risorgimento 4, I-40136 Bologna, Italy, Dipartimento di Chimica "G. Ciamician", Università di Bologna, via Selmi 2, I-40126 Bologna, Italy, and Department of Chemistry & Biochemistry, The University of Texas at Austin, Austin, Texas 78712

Received August 31, 2005

A new family of mono- and dinuclear ruthenium polypyridyl complexes containing 5-aryltetrazolate ligands such as the deprotonated form of 4-(1*H*-tetrazol-5-yl)benzonitrile (4-TBNH) and bis(1*H*-tetrazol-5-yl)benzene ($BTBH_2$) have been synthesized and thoroughly characterized. The reactivity of the mononuclear species toward different electrophiles such as H^+ and CH_3^+ has been investigated, and the effects of the resulting regioselective electrophilic attacks on the electronic and structural properties of the tetrazolate ligand have been studied by NMR (^1H, ^{13}C) spectroscopy and X-ray crystal structures. Absorption and emission spectroscopy, together with an electrochemical and UV–vis–NIR spectroelectrochemical investigation of the uncoordinated ligand and complexes, has been performed, highlighting a rather good luminescence efficiency and a poor bridge-mediated electronic communication between the metal centers of the dinuclear complexes. The electrogenerated chemiluminescence (ECL) of the dinuclear species has been explored, and for one of these, an exceptionally high ECL efficiency has been observed, comparable to that of $[Ru(bpy)_3]^{2+}$, which is considered a standard in ECL studies.

Introduction

Polypyridine derivatives of Ru(II) represent one of the most extensively studied class of coordination compounds. Interest in similar chemically stable systems stems from their peculiar electrochemical and photophysical properties,[1] which have favored the application of these molecules in several research fields such as conversion of solar energy,[2] fabrication of molecular devices,[3] DNA intercalation,[4] and protein binding.[5] Furthermore, mono- and dinuclear Ru(II) polypyridyl complexes have been widely used as ECL-luminophores.[6] Since ligand design plays a crucial role in determining and eventually improving both the light-emitting and the electron transfer performances of such systems,[7] a large number of neutral[8] and anionic[9] "actor" ligands have been

* To whom correspondence should be addressed. E-mail: palazzi@ms.fci.unibo.it (A.P.), ajbard@mail.utexas.edu (A.J.B.), massimo.marcaccio@unibo.it (M.M.).

† Dipartimento di Chimica Fisica ed Inorganica, Università di Bologna.

‡ Dipartimento di Chimica "G. Ciamician", Università di Bologna.

§ Department of Chemistry & Biochemistry, The University of Texas at Austin.

(1) (a) Balzani, V.; Scandola, F. *Supramolecular Photochemistry*; Ellis Horwood: Chichester, U.K., 1991. (b) Balzani, A.; Juris, A. *Coord. Chem. Rev.* **2001**, *211*, 97. (c) Sauvage, J.-P.; Collin, J.-P.; Chambron, J.-C.; Guillerez, S.; Coudret, C.; Balzani, V.; Barigelletti, F.; De Cola, L.; Flamigni, L. *Chem. Rev.* **1994**, *94*, 993. (d) Balzani, V.; Juris, A.; Venturi, M.; Campagna S.; Serroni, S. *Acc. Chem. Res.* **1998**, *31*, 26. (e) Slate, C. A.; Striplin, D. R.; Moss, J. A.; Chen, P.; Erickson, B. W.; Meyer, T. J. *J. Am. Chem. Soc.* **1998**, *120*, 4885.

(2) (a) Puntoriero, F.; Serroni, S.; Galletta, M.; Juris, A.; Licciardello, A.; Chiorboli, C.; Campagna, S.; Scandola, F. *ChemPhysChem* **2005**, *6*, 129. (b) Kelly, C. A.; Meyer, G. J. *Coord. Chem. Rev.* **2001**, *211*, 295. (c) Dürr, H.; Bossmann, S. *Acc. Chem. Res.* **2001**, *34*, 905. (d) Bignozzi, C. A.; Argazzi, R.; Kleverlaan, C. J. *Chem. Soc. Rev.* **2000**, *29*, 87. (e) Blanco, M.-J.; Jiménez, M. C.; Chambron, J.-C.; Heitz, V.; Linke, M.; Sauvage, J.-P. *Chem. Soc. Rev.* **1999**, *28*, 293. (f) Kalyanasundaram, K.; Gratzel, M. *Coord. Chem. Rev.* **1998**, *177*, 347. (g) De Cola, L.; Belser, P. *Coord. Chem. Rev.* **1998**, *177*, 301.

(3) (a) Balzani, V.; Credi, A.; Venturi, M. *Molecular Devices and Machines-A Journey into the Nano World*; Wiley-VCH: Weinheim, Germany, 2003. (b) Robertson, N.; McGowan, C. A. *Chem. Soc. Rev.* **2003**, *32*, 96. (c) Balzani, V.; Credi, A.; Raymo, F. M.; Stoddart, J. F. *Angew. Chem., Int. Ed.* **2000**, *39*, 3348.

(4) (a) Erkkila, K. E.; Odom, D. T.; Barton, J. K. *Chem. Rev.* **1999**, *99*, 2777 and references therein. (b) van der Schindel, K.; Garcia, F.; Kooijman H.; Spek, A. L.; Haasnoot, J. G.; Reedijk, J. *Angew. Chem., Int. Ed.* **2004**, *43*, 5668. (c) Gupta, R.; Urathamakul, T.; Williamson, N. L.; Sheil, M. A.; Aldrich-Wright, J. R.; Ralph S. R. *Chem. Commun.* **2003**, 626. (d) Xu, H.; Zheng, K.-C.; Chen, Y.; Li, Y.-Z.; Lin, L.-J.; Li, H.; Zhang, P.-X.; Ji, L.-N. *Dalton Trans.* **2003**, 2260.

10.1021/ic0514905 CCC: $33.50
Published on Web 12/16/2005

included in the coordination spheres of Ru(II) polypyridyl-metal fragments. In this context, five-membered N-heterocycle-based ligands containing imidazolyl,[10] triazolyl,[11] or pyrazolyl[12] moieties have been employed, but surprisingly, only a few examples of ruthenium[13] or osmium[14] polypyridyl complexes containing tetrazole or tetrazolate ligands have been reported so far. On the other hand, the coordination chemistry of this class of compounds[15] has been widely explored[16] and, relative to this research area, the synthesis and characterization of some of the first examples of mono- and dinuclear Fe(II) organometallic complexes containing aromatic 5-substituted tetrazolates have recently been reported.[17] In particular, the interannular conjugation effect showed by such tetrazolate ligands as well as the possibility to reversibly modulate their electronic and structural properties by a protonation−deprotonation mechanism indicated that these compounds are good candidates for incorporation into Ru(II) polypyridine complexes. Here we report studies of the synthesis, characterization, and evaluation of the main structural and electronic properties of new mono- and dinuclear complexes in which aromatic 5-substituted tetrazolates such as $[4\text{-TBN}]^-$ and $[BTB]^{2-}$ (see Chart 1) are coordinated to one or two Ru(tpy)(bpy) units.

Experimental Section

Materials. Solvents were dried and distilled under nitrogen prior to use. Unless otherwise stated, chemicals were obtained commercially (e.g. Aldrich) and used without any further purification. $Ru(tpy)Cl_3$[18] and $[Ru(tpy)(bpy)Cl][PF_6]$[19] were prepared according to literature procedures. The ligands 4-(1*H*-tetrazol-5-yl)benzonitrile (4-TBNH) and 1,4-bis(1*H*-tetrazol-5-yl)benzene ($BTBH_2$) were prepared in high yields (80% for 4-TBNH; over 95% for $BTBH_2$) according to the first established method involving 1,3 dipolar cycloaddition of azide anion (N_3^-) on the appropriate aromatic nitriles.[20]

Warning! Tetrazole derivatives are used as components for explosive mixtures.[15c] In this laboratory, the reactions described here were run on only a few grams and no problems were encountered. However, great caution should be exercised when handling or heating compounds of this type.

The formation of the anions $[4\text{-TBN}]^-$ and $[BTB]^{2-}$ was achieved by addition of equimolar amounts (2 equiv in the case of $BTBH_2$) of triethylamine to a suspension of the neutral 5-substituted tetrazoles in acetone (5 mL). The resulting colorless or pale yellow solutions were used without any further purification. Throughout this paper, the percentage yields of the product complexes are referred to the molar quantity of the starting $[Ru(tpy)(bpy)Cl][PF_6]$.

Synthesis of the Mononuclear Complex $[Ru(4\text{-TBN})][PF_6]$. $[Ru(tpy)(bpy)Cl][PF_6]$ (0.500 g, 0.74 mmol) was dissolved in deaerated acetone (15 mL) in a 100 mL round-bottom flask protected from light. A slight excess (1.1 equiv) of $AgPF_6$ was added, and the mixture was stirred with reflux for 4 h. The reaction mixture was filtered through a Celite pad, and the filtrate was added dropwise to an acetone (10 mL) solution of the tetrazolate ligand $[4\text{-TBN}]^-$ (0.8 mmol). Once the addition was complete, the deep red solution was stirred at reflux temperature overnight. The mixture was then cooled to rt (room temperature), concentrated to about 20 mL, added to 10 mL of an aqueous solution containing ca. 0.5

(5) (a) Yang, X.-J.; Drepper, F.; Wu, B.; Sun, W.-H.; Haehnel, W.; Janiak, C. *Dalton Trans.* **2005**, 256. (b) Karidi, K.; Garoufis, A.; Hadjiliadis, N.; Reedijk, J. *Dalton Trans* **2005**, 728. (c) Hofmeier, H.; Pahnke, J.; Weidl, C. H.; Schubert, U. S. *Biomacromolecules* **2004**, *5*, 2055 and references therein.

(6) (a) Richter, M. M. *Chem. Rev.* **2004**, *104*, 3003. (b) Miao, W. J.; Bard, A. J. *Anal. Chem.* **2004**, *76*, 7109. (c) Welter, S.; Brunner, K.; Hofstraat, J. W.; De Cola, L. *Nature* **2003**, *421*, 54. (d) Liu, C.-Y.; Bard, A. J. *J. Am. Chem. Soc.* **2002**, *124*, 4190. (e) Liu, C.-Y.; Bard, A. J. *Acc. Chem. Res.* **1999**, *32*, 235 and references therein.

(7) (a) Elsevier, C. J.; Reedijk, J.; Walton, P. H.; Ward, M. D. *Dalton Trans.* **2003**, 1869. (b) Demadis, K. D.; Hartshorn, C. M.; Meyer, T. J. *Chem. Rev.* **2001**, *101*, 2655. (c) Kaim, W.; Klein, A.; Glöckle, M. *Acc. Chem. Res.* **2000**, 33, 755 and references therein.

(8) (a) Balzani, V.; Juris, A.; Venturi, M.; Campagna, S.; Serroni, S. *Chem. Rev.* **1996**, *96*, 759. (b) Newkome, G. R.; Patri, A. K.; Holder, E.; Schubert, U. S. *Eur. J. Org. Chem.* **2004**, 235. (c) Medlycott E. A.; Hanan, G. S. *Chem. Soc. Rev.* **2005**, *34*, 133. (d) Hofmeier, H.; Schubert, U. S. *Chem. Soc. Rev.* **2004**, *33*, 373. (e) Zong, R.; Thummel, R. P. *J. Am. Chem. Soc.* **2004**, *126*, 10800. (f) Bergman, S. D., Golberg, I.; Barbieri, A.; Barigelletti, F.; Kol, M. *Inorg. Chem.* **2004**, *43*, 2355 and references therein.

(9) (a) Fraysse, S.; Coudret, C.; Launay, J. P. *J. Am. Chem. Soc.* **2003**, *125*, 5880. (b) Launay, J. P. *Chem. Soc. Rev.* **2001**, *30*, 386. (c) Sondaz, E.; Jaud, J.; Launay, J. P.; Bonvoisin, J. *Eur. J. Inorg. Chem.* **2002**, 1924. (d) Sondaz, E.; Gourdon, A.; Launay, J. P.; Bonvoisin, J. *Inorg. Chim. Acta* **2001**, *316*, 79. (e) Crutchley, R. J. *Coord. Chem. Rev.* **2001**, *219*, 125 and references therein.

(10) (a) Shavaleev, N. M.; Bell, Z. R.; Easun, T. L.; Rutkaite, R.; Swanson, L.; Ward, M. D. *Dalton Trans.* **2004**, 3678. (b) Haga, M.-A.; Ali, Md. M.; Koseki, S.; Fujimoto, K.; Yoshimura, A.; Nozaki, K.; Ohno, T.; Nakajima, K.; Stufkens, D. J. *Inorg. Chem.* **1996**, *35*, 3335. (c) Hatzidimitriou, A.; Gourdon, A.; Devillers, J.; Launay, J. P.; Mena, E.; Amouyal, E. *Inorg. Chem.* **1996**, *35*, 2212.

(11) (a) Browne, W. R.; O'Boyle, N. M.; Henry, W.; Guckian, A. L.; Horn, S.; Fett, T.; O'Connor, C. M.; Duati, M.; De Cola, L.; Coates, C. G.; Ronayne, K. L.; McGarvey, J. J.; Vos, J. G. *J. Am. Chem. Soc.* **2005**, *127*, 1229. (b) Browne, W. R.; Hesek, D.; Gallagher, J. F.; O'Connor, C. M.; Killeen, J. S.; Aoki, F.; Ishida, H.; Inoue, Y.; Villani, C.; Vos, J. G. *Dalton Trans.* **2003**, 2597. (c) Klingele, M. H.; Brooker, S. *Coord. Chem. Rev.* **2003**, *241*, 119. (d) Fanni, S.; Keyes, T. E.; O'Connor, C. M.; Hughes, H.; Wang, R.; Vos, J. G. *Coord. Chem. Rev.* **2000**, *208*, 77 and references therein.

(12) (a) Chanda, N.; Sarkar, B.; Kar, S.; Fiedler, J.; Kaim, W.; Lahiri, G. K. *Inorg. Chem.* **2004**, *43*, 5128. (b) Sens, C.; Rodriguez, M.; Romero, I.; Llobet, A.; Parella, T.; Benet-Buchholz, J. *Inorg. Chem.* **2003**, *42*, 8385. (c) Laye, R. H.; Couchman, S. M.; Ward, M. D. *Inorg. Chem.* **2001**, *40*, 4089.

(13) (a) Duati, M.; Tasca, S.; Lynch, F. C.; Bohlen, H.; Vos, J. G.; Stagni, S.; Ward, M. D. *Inorg. Chem.* **2003**, *42*, 8377. (b) Massi, M.; Cavallini, M.; Stagni, S.; Palazzi, A.; Biscarini, F. *Mater. Sci. Eng., C* **2003**, *23*, 923. (c) Downard, A. J.; Steel, P. J.; Steenwijk, J. *Aust. J. Chem* **1995**, *48*, 1625.

(14) (a) Demadis, K. D.; Meyer, T. J.; White, P. S. *Inorg. Chem.* **1998**, *37*, 3610. (b) Demadis, K. D.; El-Samanody, E.-S.; Meyer, T. J.; White, P. S. *Inorg. Chem.* **1998**, *37*, 838.

(15) The rapid development of tetrazole-based compounds is mostly associated with the wide scale employment of these heterocycles in several areas of research connected to medicinal science; see: (a) Fürmeier, S.; Metzger, J. O. *Eur. J. Org. Chem.* **2003**, 885. (b) Herr, R. J. *Bioorg. Med. Chem.* **2002**, *10*, 3379. (c) Butler, R. N. In *Comprehensive Heterocyclic Chemistry II*; Storr, R. C., Ed.; Tetrazoles, Vol.4; Pergamon Press: Oxford, U.K., 1996; pp 621−678 and references therein. (d) Adamantini, A.; Beleggia, R.; Fringuelli, F.; Pizzo, F.; Vaccaro, L. *J. Org. Chem.* **2004**, *69*, 2896. (e) Demko, Z. P.; Sharpless, K. B. *J. Org. Chem.* **2001**, *66*, 7945. (f) Koguro, K.; Oga, T.; Mitsui, S.; Orita, R. *Synthesis* **1998**, 910.

(16) (a) Moore, D. S.; Robinson, S. D. *Adv. Inorg. Chem.* **1988**, *32*, 171 and references therein. (b) He, F.; Tong, M. L.; Yu, X. L.; Chen, X. M. *Inorg. Chem.* **2005**, *44*, 559. (c) Chang, C. W.; Lee, G. H. *Organometallics* **2003**, *22*, 3107. See also: (d) Kukushkin, V. Yu.; Pombeiro, A. J. L. *Chem. Rev.* **2002**, *102*, 1771 and references therein.

(17) (a) Palazzi, A.; Stagni, S. *J. Organomet. Chem.* **2005**, *690*, 2052. (b) Palazzi, A.; Stagni, S.; Monari, M.; Selva, S. *J. Organomet. Chem.* **2003**, *669*, 135. (c) Palazzi, A.; Stagni, S.; Bordoni, S.; Monari, M.; Selva, S. *Organometallics* **2002**, *21*, 3774.

(18) Sullivan, B. P.; Calvert, J. M.; Meyer, T. J. *Inorg. Chem.* **1980**, *19*, 1404.

(19) Rasmussen, S. C.; Ronco, S. E.; Mlsna, D. A.; Billadeau, M. A.; Pennington, W. T.; Kolis, J. W.; Petersen, J. D. *Inorg. Chem.* **1995**, *34*, 821.

(20) Finnegan, W. A., Henry, R. A., Lofquist, R. *J. Am. Chem. Soc.* **1958**, *80*, 3908.

Chart 1. Ligands, Complexes, and Acronyms Used in This Work

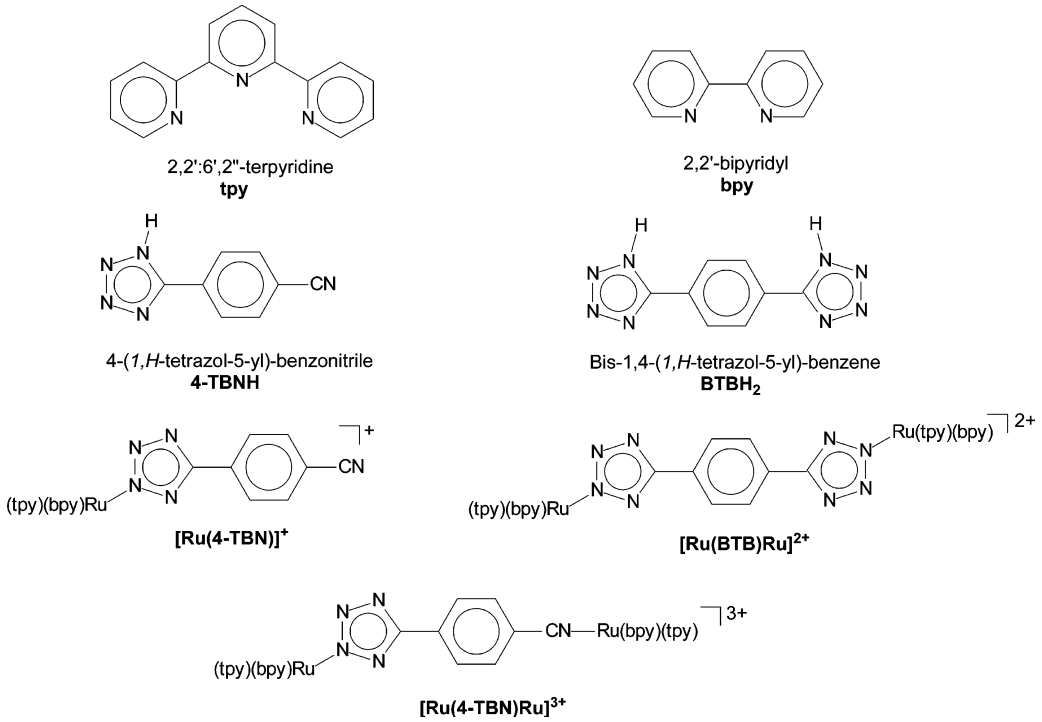

g of NH_4PF_6, and extracted with dichloromethane (3 × 20 mL) until the aqueous phase became colorless. The organic layers were dried over $MgSO_4$, and the solvent was removed in vacuo. The red mixture was redissolved in a minimal quantity of dry acetone and added to a copious amount of diethyl ether, causing the precipitation of a crude product which was collected by suction filtration and purified by alumina filled column chromatography with acetone/toluene mixtures as the eluent. Three bands were eluted in the following order: a purple band identified as the starting [Ru(tpy)(bpy)Cl][PF_6] (acetone/toluene 1/1 (v/v) as the eluent); the target mononuclear complex as a deep red fraction (acetone/toluene 1.5/1); the final brown band consisting of small amount of the dinuclear species [Ru(4-TBN)Ru][PF_6]$_3$ eluted with pure acetone. The fractions containing the mononuclear compound were evaporated to dryness, affording [Ru(4-TBN)][PF_6] (0.360 g, 60%) as a deep red microcrystalline powder. ESI-MS: *m*/*z* 661, [M − PF_6^-]$^+$. Suitable crystals for X-rays analysis were obtained by the slow diffusion of diethyl ether into a dichloromethane solution of the complex, which crystallized as [Ru(4-TBN)][PF_6]·2CH_2Cl_2. Anal. Calcd for $C_{35}H_{27}Cl_4F_6N_{10}PRu$·2$CH_2Cl_2$ (M_r = 975.51): C, 43.09; H, 2.80; N, 14.36. Found: C, 42.95; H, 2.92; N, 14.25.

Methylation Reaction. [Ru(4-TBN)][PF_6] (0.100 g, 0.12 mmol) was dissolved in dichloromethane (10 mL) under argon atmosphere, and the resulting deep red solution was cooled to −50 °C; then $CH_3OSO_2CF_3$ (1 mL, 0.124 M in dichloromethane, 0.124 mmol) was added dropwise. After 30 min, the red mixture was allowed to warm to rt and stirred for additional 6 h. Evaporation of the solvent afforded a red oily residue which was dissolved into a minimal amount of acetonitrile and added to 10 mL of an aqueous solution containing ca. 0.5 g of NH_4PF_6. The resulting mixture was extracted with dichloromethane (3 × 20 mL) until the aqueous phase became colorless. The organic layers were dried over $MgSO_4$ and the solvent was removed in vacuo, affording a red solid which was identified as the methylated product [Ru(4-(Me)TBN)][PF_6]$_2$ (0.090 g, 78%). ESI-MS: *m*/*z* 338, [M − 2PF_6^-]$^{2+}$. Suitable crystals for X-rays analysis were obtained by the slow diffusion of diethyl ether into an acetonitrile solution the complex, which crystallized as [Ru(4-(Me)TBN)][PF_6]$_{1.56}$[SO_3CF_3]$_{0.44}$ showing the presence of residual triflate anion. Anal. Calcd for $C_{34.44}H_{26}F_{10.68}N_{10}O_{1.33}P_{1.56}RuS_{0.44}$ (M_r = 967.48): C, 42.75; H, 2.71; N, 14.48. Found: C, 42.88; H, 2.84; N, 14.05.

Protonation Reaction. The deep red solution obtained by dissolving under argon atmosphere a 0.100 g aliquot of the starting complex [Ru(4-TBN)][PF_6] (0.12 mmol) in dichloromethane (10 mL) was cooled to −50 °C. Then a slight excess (1.1 equiv) of $HOSO_2CF_3$ (1 mL, 0.136 M in dichloromethane, 0.136 mmol) was added dropwise. After 30 min, the reaction mixture was allowed to warm to rt and stirred for additional 6 h. The solvent was the removed in vacuo, affording a red oily residue which was redissolved in acetonitrile (5 mL), and added to a copious amount of diethyl ether, causing the precipitation of a microcrystalline powder. The mixture was maintained under argon atmosphere and filtered through a glass frit, affording a deep orange solid which analyzed well as [Ru(4-(H)TBN)][SO_3CF_3]$_2$ (0.085 g, 90%). ESI-MS: *m*/*z* 331, [M − 2$SO_3CF_3^-$]$^{2+}$. Suitable crystals for X-ray determination were obtained by the slow diffusion of diethyl ether into an acetonitrile solution of the protonated complex, which crystallized as [Ru(4-(H)TBN)][SO_3CF_3]$_2$·CH_3CN·H_2O. Anal. Calcd for $C_{37}H_{29}F_6N_{11}O_7RuS_2$ (M_r = 1018.90): C, 43.62; H, 2.87; N, 15.12. Found: C, 44.00; H, 2.98; N, 15.75.

Preparation of the Dinuclear Complexes [Ru(4-TBN)Ru][PF_6]$_3$ and [Ru(BTB)Ru][PF_6]$_2$. The reactive species obtained from the Ag(I)-mediated chloride extraction of [Ru(tpy)(bpy)Cl][PF_6] (0.250 g, 0.37 mmol) was dissolved in 15 mL of deareated acetone and successively combined with an acetone solution (5 mL) containing 0.5 equiv (calculated with respect to the starting [Ru(tpy)(bpy)Cl][PF_6]) of the appropriate tetrazolate ligand. Then the deep red mixture was stirred at reflux temperature for 15 h, and a workup procedure analogous to that reported above for the mononuclear compound afforded a crude product which was purified by alumina filled column chromatography. The dinuclear complex [Ru(4-TBN)Ru][PF_6]$_3$ (0.110 g, 37%) was eluted as the final product with pure acetone. ESI-MS: *m*/*z* 384, [M − 3PF_6^-]$^{3+}$. Anal. Calcd for $C_{58}H_{42}N_{15}F_{18}P_3Ru_2$: C, 43.92; H, 2.67; N, 13.25.

Found: C, 44.20; H, 2.85; N, 13.55. An analogous procedure was followed for the preparation of the symmetrically bridged species $[Ru(BTB)Ru][PF_6]_2$. In this latter case, the alumina filled column chromatography of the crude product afforded the target dinuclear complex $[Ru(BTB)Ru][PF_6]_2$ (0.150 g, 27%) as a deep red-brown fraction by elution with a 2/1 (v/v) acetone/toluene mixture. ESI-MS: *m/z*: 597, $[M - 2PF_6]^{2+}$. Anal. Calcd for $C_{58}H_{42}N_{18}F_{12}P_2Ru_2$: C, 46.97; H, 2.85; N, 17.00. Found: C, 47.20; H, 2.95; N, 17.30.

Instrumentation and Procedures. All the obtained complexes were characterized by elemental analysis and spectroscopic methods. Elemental analyses were performed on a ThermoQuest Flash 1112 Series EA instrument. ESI-mass spectra were performed on a Waters ZQ-4000 instrument; acetonitrile was used as the solvent. The routine NMR spectra (^{1}H, ^{13}C) were always recorded using a Varian Mercury Plus 400 instrument (^{1}H, 400.1; ^{13}C, 100 MHz). The spectra were referenced internally to residual solvent resonance and were recorded at 298 K for characterization purposes. Bidimensional ^{1}H,^{13}C correlation spectra were measured via gs-HSQC and gs-HMBC experiments,[21] whereas ^{1}H,^{1}H correlations were determined by gs-COSY experiments.[22]

Electrochemical and Spectroelectrochemical Measurements. Tetraethylammonium tetrafluoborate (TEATFB; from Fluka) and tetrabutylammonium hexafluorophosphate (TBAH; from Fluka) were used as received as supporting electrolyte. Dry vacuum distilled *N*,*N*-dimethylformamide (DMF) was purified using sodium anthracenide to remove any traces of water and oxygen, according to the method of Aoyagui and co-workers.[23] Acetonitrile (ACN), after being refluxed over CaH_2, was distilled under vacuum at room temperature with a high refluxing ratio, utilizing a 1 m length distillation column filled with glass rings, and it was stored in a specially designed Schlenk flask over 3 Å activated molecular sieves, protected from light. The solvent was distilled via a closed system into an electrochemical cell containing the supporting electrolyte and the species under examination, soon before performing the experiment. All the other chemicals were of reagent grade. Electrochemical experiments were carried out in an airtight single-compartment cell described elsewhere,[24] by using platinum as working and counter electrodes and a silver spiral as a quasi-reference electrode. The drift of the quasi-reference electrode was negligible for the time required by an experiment. All the $E_{1/2}$ potentials have been directly obtained from cvc's as average of the cathodic and anodic peak potentials for one-electron peaks and by digital simulation for those processes closely spaced in multi-electron voltammetric peaks. The $E_{1/2}$ values, referred to an aqueous saturated calomel electrode (SCE), have been determined by adding at the end of each experiment ferrocene as an internal standard and measuring them with respect to the ferrocenium/ferrocene couple standard potential. The cell containing the supporting electrolyte and the electroactive compound was dried under vacuum at 100−110 °C for at least 60 h before each experiment. The pressure measured in the electrochemical cell prior to performing the trap-to-trap distillation of the solvent was typically $(1-2) \times 10^{-5}$ mbar. Voltammograms were recorded with an AMEL model 552 potentiostat controlled by an AMEL model 568 programmable function generator. The potentiostat was interfaced to a Nicolet model 3091 digital oscilloscope, and the data were transferred to a personal computer by the program Antigona.[25] The minimization of the uncompensated resistance effect in the voltammetric measurements was achieved by the positive-feedback circuit of the potentiostat. Digital simulation of the cyclic voltammetric curves was carried out either by Antigona or DigiSim 3.0. The spectroelectrochemical experiments have been carried out using a quartz OTTLE cell with a 0.03 cm path length. Temperature control was achieved by a special cell holder with quartz windows, in which two nitrogen fluxes (one at room temperature and the other at low temperature) were regulated by two needle valves. All the spectra have been recorded by a Cary 5. All the experimental details for the spectroelectrochemical setup have been reported elsewhere.[26] All fluorescence spectra were recorded on a Fluorolog-3 spectrofluorometer (ISA-Jobin Yvon Hariba, Edison, NJ) using a slit width of 1 nm and a resolution of 1.5 nm. All UV−visible spectra were recorded on a Milton Roy Spectronic 3000 array spectrophotometer. The absorbance and fluorescence spectra of the complexes were obtained with a 40 μM acetonitrile (ACN) solution, and the relative fluorescence efficiency was calibrated with $Ru(bpy)_3^{2+}$ as a standard ($\lambda_{exc} = 500$ nm). ECL measurements were obtained as previously reported[27] with 1 mM $[Ru(BTB)Ru]^{2+}$ or $[Ru(4\text{-}TBN)Ru]^{3+}$ ACN solutions, 0.1 M in supporting electrolyte TBAH (from Fluka). To generate the annihilation reaction, the working electrode was pulsed between the first oxidation and reduction peak potentials of $[Ru(BTB)Ru]^{2+}$ and $[Ru(4\text{-}TBN)Ru]^{3+}$ with a pulse width of 0.1 s. The resulting emission spectra were obtained with a charged-coupled device (CCD) camera (Photometrics CH 260, Photometrics-Roper Scientific, Tucson, AZ) that was cooled to −100 °C. Integration times were 4 min. The CCD camera and grating system were calibrated with a mercury lamp prior to each measurement. ECL yields were determined against the standard, i.e., $Ru(bpy)_3^{3-}$–$Ru(bpy)_3^-$ ECL system in ACN solution containing 0.1 M TBAH (with $\phi_{ecl} = 0.05$),[28] taking also into account the differences in the charges passed through the studied solution. In a given solution, two or three records were made to check the temporal stability of the system studied. Since the compounds can undergo several reduction and oxidation processes, scans with different limits were performed over the available potential window to include 2, 3, or 4 redox processes.

X-ray Crystallography. Crystal data and collection details are reported in Table 1. The diffraction experiments were carried out on a Bruker APEX II diffractometer (for $[Ru(4\text{-}TBN)][PF_6]\cdot 2CH_2Cl_2$ and $[Ru(4\text{-}(H)TBN)][CF_3SO_3]_2\cdot CH_3CN\cdot H_2O$) and on a Bruker SMART 2000 diffractometer (for $[Ru(4\text{-}(Me)TBN)][PF_6]_{1.56}[CF_3SO_3]_{0.44}$), equipped with a CCD detector and using Mo Kα radiation. Data were corrected for Lorentz polarization and absorption effects (empirical absorption correction SADABS).[29] Structures were solved by direct methods and refined by full-matrix least-squares on the basis of all data using F^2.[30] H atoms were placed in calculated positions, except H(9n) in $[Ru(4\text{-}(H)TBN)][CF_3SO_3]_2\cdot CH_3CN\cdot H_2O$, which was located in the Fourier map and refined with the N(9)−H(9n) distance restrained to 0.86 Å; conversely, it has not been possible to locate the H atoms for the water molecule in $[Ru(4\text{-}(H)TBN)][CF_3SO_3]_2\cdot CH_3CN\cdot H_2O$. H atoms were treated isotropi-

(21) Wilker, W.; Leibfritz, D.; Kerssebaum, R.; Beimel, W. *Magn. Reson. Chem.* **1993**, *31*, 287.
(22) Hurd, R. E. *J. Magn. Reson.* **1990**, *87*, 422.
(23) Saji, T.; Yamada, T.; Aoyagui, S. *J. Electroanal. Chem.* **1975**, *61*, 147.
(24) Marcaccio, M.; Paolucci, F.; Paradisi, C.; Roffia, S.; Fontanesi, C.; Yellowlees, L. J.; Serroni, S.; Campagna, S.; Denti, G.; Balzani, V. *J. Am. Chem. Soc.* **1999**, *121*, 10081.
(25) Antigona was developed by Dr. Loic Mottier.
(26) Lee, S.-M.; Kowallick, R.; Marcaccio, M.; McCleverty, J. A.; Ward, M. D. *J. Chem. Soc., Dalton Trans.* **1998**, 3443.
(27) McCord, P.; Bard, A. J. *J. Electroanal. Chem.* **1991**, *318*, 91
(28) Wallace, W. L.; Bard, A. J. *J. Phys. Chem.* **1979**, *83*, 1350.
(29) Sheldrick, G. M. *SADABS, Program for Empirical Absorption Correction*; University of Göttingen: Göttingen, Germany, 1996.
(30) Sheldrick, G. M. *SHELX97-Program for the refinement of Crystal Structure*; University of Göttingen: Göttingen, Germany, 1997.

Table 1. Crystal Data and Experimental Details for $[Ru(4\text{-}TBN)][PF_6]\cdot 2CH_2Cl_2$, $[Ru(4\text{-}(Me)TBN)][PF_6]_{1.56}[CF_3SO_3]_{0.44}$, and $[Ru(4\text{-}(H)TBN)][CF_3SO_3]_2\cdot CH_3CN\cdot H_2O$

param	$[Ru(4\text{-}TBN)[PF_6]\cdot 2CH_2Cl_2$	$[Ru(4\text{-}(Me)TBN)][PF6]_{1.56}[CF_3SO_3]_{0.44}$	$[Ru(4\text{-}(H)TBN)][CF_3SO_3]2\cdot CH_3CN\cdot H_2O$
Formula	$C_{35}H_{27}Cl_4F_6N_{10}PRu$	$C_{34.44}H_{26}F_{10.68}N_{10}O_{1.33}P_{1.56}RuS_{0.44}$	$C_{37}H_{29}F_6N_{11}O_7RuS_2$
fw	975.51	967.48	1018.90
T, K	100(2)	293(2)	296(2)
λ, Å	0.710 73	0.710 73	0.710 73
cryst system	monoclinic	monoclinic	triclinic
space group	$P2_1/c$	$P2_1/c$	$P\bar{1}$
a, Å	8.5520(4)	14.294(3)	9.392(4)
b, Å	21.0605(10)	17.306(4)	10.915(4)
c, Å	21.1224(9)	16.038(3)	20.692(8)
α, deg	90	90	84.953(6)
β, deg	92.827(2)	101.22(3)	88.306(6)
γ, deg	90	90	83.028(6)
cell vol, Å^3	3799.7(3)	3891.5(14)	2096.9(14)
Z	4	4	2
D_c, g cm^{-3}	1.705	1.651	1.614
μ, mm^{-1}	0.809	0.587	0.563
F(000)	1952	1935	1028
cryst size, mm	0.22 × 0.14 × 0.13	0.18 × 0.14 × 0.11	0.19 × 0.14 × 0.11
θ limits, deg	1.93−25.03	1.45−25.03	1.89−25.03
reflcns collcd	23 704	34 357	18 484
indepndt reflcns	6698 (R_{int} = 0.0402)	6859 (R_{int} = 0.1020)	7359 (R_{int} = 0.0959)
data/restraints/params	6698/3/512	6859/58/606	7359/207/581
goodness on fit on F^2	1.041	1.050	0.972
R_1 ($I > 2\sigma(I)$)	0.0412	0.0534	0.0734
wR_2 (all data)	0.1076	0.1388	0.2144
largest diff peak and hole, e·Å^{-3}	1.143/−1.036	1.163/−0.734	0.870/−1.486

Scheme 1. Synthetic Pathway Followed for the Preparation of Tetrazolate Complexes

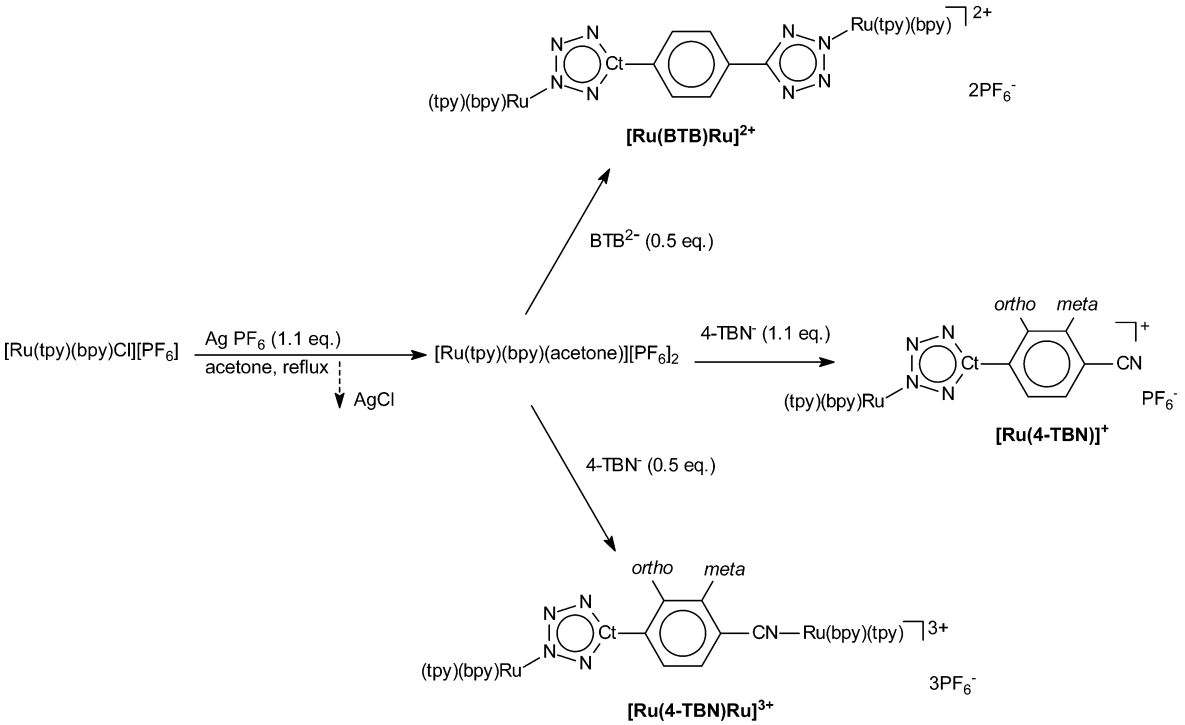

cally using the 1.2-fold U_{iso} value of the parent atom except methyl protons, which were assigned the 1.5-fold U_{iso} value of the parent C atom. All non-hydrogen atoms were refined with anisotropic displacement parameters, unless otherwise stated. One of the two CH_2Cl_2 molecules in $[Ru(4\text{-}TBN)][PF_6]\cdot 2CH_2Cl_2$ is disordered over two positions. Moreover, substitutional disorder is present in $[Ru(4\text{-}(Me)TBN)][PF_6]_{1.56}[CF_3SO_3]_{0.44}$, where the site of one of the two anions is partially occupied by PF_6^- and partially by $CF_3SO_3^-$. Attempts to refine the structure using only one type of anion resulted in a lower fitting of the model with the experimental data with high residual electron density nearby the anion. Disordered atomic positions were split and refined using similar distance and similar U restraints and one occupancy parameter/disordered group.

Results and Discussion

Synthesis, NMR, Structural Characterization, and Reactivity of Complexes. The synthetic procedure for the preparation of the target mono- and dinuclear complexes $[Ru(4\text{-}TBN)]^+$, $[Ru(4\text{-}TBN)Ru]^{3+}$, and $[Ru(BTB)Ru]^{2+}$ (Scheme 1) involved the preliminary reaction of the ruthenium precursor $[Ru(tpy)(bpy)Cl][PF_6]$ with a slight molar excess

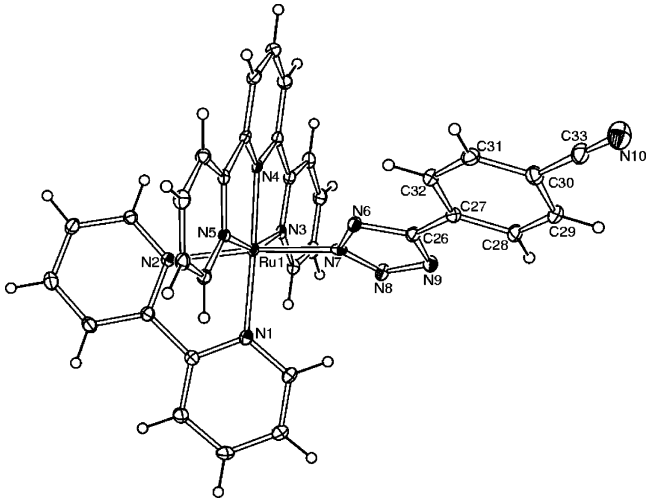

Figure 1. Molecular structure of the cation $[Ru(4\text{-}TBN)]^+$, with key atoms labeled. Displacement ellipsoids are at 30% probability level.

Table 2. Selected Bond Lengths (Å) and Angles (deg) for $[Ru(4\text{-}TBN)]^+$, $[Ru(4\text{-}(Me)TBN)]^{2+}$, and $[Ru(4\text{-}(H)TBN)]^{2+}$

param	$[Ru(4\text{-}TBN)]^+$	$[Ru(4\text{-}(Me)TBN)]^{2+}$	$[Ru(4\text{-}(H)TBN)]^{2+}$
Ru(1)−N(1)	2.076(3)	2.079(4)	2.070(6)
Ru(1)−N(2)	2.063(3)	2.047(4)	2.050(6)
Ru(1)−N(3)	2.069(3)	2.060(4)	2.071(6)
Ru(1)−N(4)	1.962(3)	1.975(4)	1.965(5)
Ru(1)−N(5)	2.074(3)	2.067(4)	2.065(6)
Ru(1)−N(7)	2.086(3)	2.067(4)	2.084(6)
N(6)−N(7)	1.332(4)	1.352(5)	1.347(8)
N(7)−N(8)	1.309(4)	1.299(5)	1.307(8)
N(8)−N(9)	1.339(4)	1.341(5)	1.324(9)
N(9)−C(26)	1.344(5)	1.330(6)	1.337(9)
N(6)−C(26)	1.337(5)	1.325(6)	1.316(9)
C(26)−C(27)	1.472(5)	1.462(7)	1.480(10)
N(6)−N(7)−N(8)	113.1(3)	111.5(4)	111.8(6)
N(7)−N(8)−N(9)	107.0(3)	105.5(4)	105.1(6)
N(8)−N(9)−C(26)	105.4(3)	109.3(4)	109.7(6)
N(9)−C(26)−N(6)	112.1(3)	108.4(4)	108.4(7)
C(26)−N(6)−N(7)	102.4(3)	105.3(4)	105.1(6)
C(30)−C(33)−N(10)	178.3(5)	176.9(9)	174.0(12)

of a silver salt, such as $AgPF_6$, in refluxing acetone. The removal of the precipitated AgCl afforded a deep red filtrate, probably containing the solvato complex [Ru(tpy)(bpy)(acetone)][PF_6]$_2$, which was thoroughly combined with an acetone solution of the desired 5-substituted tetrazolate ligand $[4\text{-}TBN]^-$ or $[BTB]^{2-}$.

The reaction mixtures was stirred at reflux for 10−15 h, and the target complexes were all purified by alumina filled column chromatography. The confirmation of the composition of each of the target mono- and dinuclear complexes was provided by the positive ion ESI mass spectra. Moreover, the molecular structure of $[Ru(4\text{-}TBN)]^+$ has been confirmed by X-ray diffraction studies (Figure 1, Table 2). The molecule is composed of a Ru(tpy)(bpy) fragment to which the 5-substituted tetrazolate ligand is N-2 coordinated. The bonding parameters for the former parallel very well the ones reported for other complexes containing the Ru(tpy)(bpy) unit.[5a,9c−d] In particular, the bond distance of ruthenium to the central tpy nitrogen [Ru(1)−N(4) = 1.962(3) Å] is ca. 0.1 Å shorter than the other Ru−N distances (2.06−2.09 Å), and this is typical of the tpy coordination to ruthenium and osmium complexes.[8a] The tetrazolate ring is flat (deviations from the average plane in the range +0.003 to −0.004 Å) and almost coplanar with the bonded aromatic ring [dihedral angle N(6)−C(26)−C(27)−C(32) = 7.3(6)°]. A similar conformation of the 5-substituted tetrazolate ligand had been previously observed in the iron complex [CpFe(CO)(P(OCH_3)$_3$)($N_4CC_6H_4CN$)][17c] and clearly indicates interring conjugation within the ligand. The formation of C−H···π and π···π interactions in the crystals of [Ru(4-TBN)][PF_6]·2CH_2Cl_2 is mainly hampered by the separation action of the PF_6^- anion and the two CH_2Cl_2 molecules. Only few interactions are, therefore, present, and they can be classified as weak on the basis of the rather long centroid−centroid distances (>4.4 Å) and the large slip angles (>40°).[31]

Chart 2. N-1 and N-2 Coordination Isomers of Tetrazolate Complexes

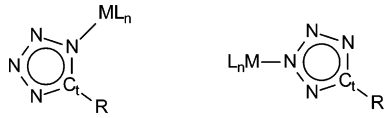

N-1 isomer N-2 isomer

The NMR characterization of all the mononuclear species has been accomplished with the use of ^{1}H gs-COSY, ^{1}H,^{13}C gs-HSQC, and ^{1}H,^{13}C gs-HMQC two-dimensional techniques, leading to the clear distinction of the resonances due to the 5-substituted tetrazolate ligand (see Table 3) from those due to the tpy and bpy moieties. Complete NMR (^{1}H, ^{13}C) data and spectra are reported in the Supporting Information.

The complexation reaction of tetrazolate salts can lead to the formation of different coordination isomers (Chart 2).

In the particular case of 5-aryl- or 5-pyridyl-substituted tetrazolate ligands, the ^{13}C NMR resonance of the tetrazolate carbon (Ct) represent a reliable parameter to determine whether the metal fragment is N-1 [δ(Ct) = 151−155 ppm] or N-2 coordinated [δ(Ct) = 161−165 ppm] to the tetrazolate moiety (see Chart 2).[17,32] Relative to $[Ru(4\text{-}TBN)]^+$, the exclusive formation of the less hindered N-2 coordinated isomer is indicated by the presence of a single tetrazolate (Ct; see Table 3) carbon resonance at 163.4 ppm, which falls in the chemical shifts range (161−165 ppm) typical of N-2 coordinated tetrazolate complexes[17,32] and of N-2 methyl derivatives of organic 5-aryltetrazoles.[33] In addition, the presence of interannular conjugation in the 5-aryltetrazolate ligand of complex $[Ru(4\text{-}TBN)]^+$ is indicated by the chemical shifts separation [$\Delta(\delta(C_{meta}) - \delta(C_{ortho})) = 6.4$ ppm] between the carbons *meta* and *ortho* (relative to the tetrazole group; see Scheme 1) of the benzonitrile ring. The magnitude of this parameter, which has been introduced by Butler and coworkers[33] for determining the extent of interannular conjugation in a series of organic 5-aryltetrazoles, is even greater than what we recently reported [$\Delta(\delta(C_{meta})-\delta(C_{ortho})) = 5.1$ ppm] in the case of the analogue organometallic complex [Cp(CO)(P(OMe)$_3$)$FeN_4CC_6H_4CN$],[17c] the structural deter-

(31) Janiak, C. *Dalton Trans.* **2000**, 3885.
(32) (a) Jackson, W. G.; Cortez, S. *Inorg. Chem.* **1994**, *33*, 1921 and references therein. (b) Takach, N. E.; Holt, E. M.; Alcock, N. W.; Henry, R. A.; Nelson, J. H. *J. Am. Chem. Soc.* **1980**, *102*, 2968.
(33) Butler, R. N. In *Comprehensive Heterocyclic Chemistry*; Potts, K. T., Ed.; Tetrazoles; Pergamon Press: Oxford, U.K., 1984; Vol. 5, pp 791−838 and references therein.

Table 3. Selected ^{1}H and ^{13}C NMR Data[a] for All the Complexes Reported in This Paper with Atom Labeling Presented in Scheme 1

complex	δ(Ct)	$\delta(C_{meta})$	$\delta(C_{ortho})$	$\Delta[\delta(C_{meta})-\delta(C_{ortho})]$	$\delta(H_{ortho})$	$\delta(H_{meta})$
$[Ru(4\text{-}TBN)]^{+}$	163.4	133.5	127.2	6.3	7.86	7.63
$[Ru(4\text{-}(H)TBN)]^{2+}$	156.6	134.3	128.9	5.4	7.85	7.85
$[Ru(4\text{-}(Me)TBN)]^{2+}$	156.4	134.0	130.5	3.5	7.62	7.85
$[Ru[4\text{-}TBN]Ru]^{3+}$	163.1	134.7	128.3	6.4	*b*	*b*
$[Ru[BTB]Ru]^{2+}$	164.3	126.8	126.8		7.64	7.64

[a] CD_3CN as solvent, room temperature, chemical shifts expressed in ppm. [b] Overlapping with bpy and tpy resonances.

Scheme 2. (a) Methylation Reactions and (b) Selected ^{13}C NMR Signals of the Methylated Compound $[Ru(4\text{-}Me)TBN]^{2+}$ (Right) Compared to Those of the Starting Complex $[Ru(4\text{-}TBN)]^{+}$ (Left)

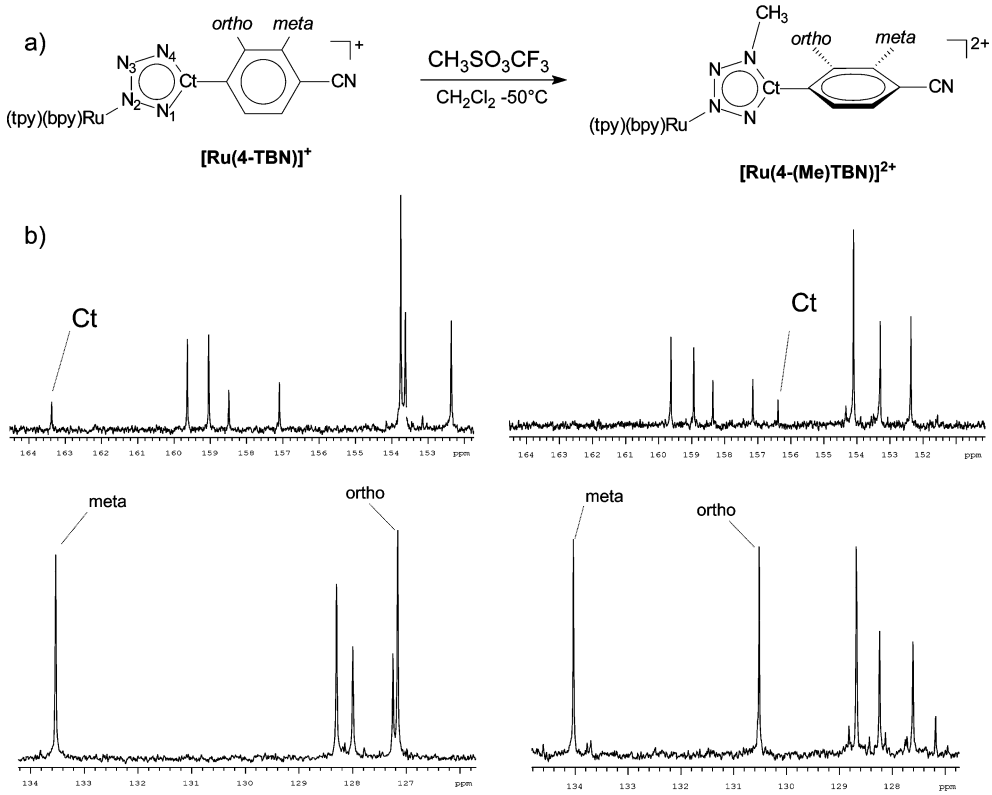

mination of which showed the tetrazolate moiety and the phenyl ring to be coplanar.

Reactivity toward Electrophiles. The presence of three imine-type nitrogen atoms in the N-2 coordinated five-membered ring of the 5-substituted tetrazolate ligands offers different sites which could undergo alkylation and/or protonation reactions. In particular, electrophilic additions onto organometallic complexes such as $[Cp(CO)(L)FeN_4CC_6H_4\text{-}CN]$ (L = CO, PPh_3, $P(OMe)_3$)[17c] were reported to cause significant modifications to the structural and electronic properties of the coordinated 5-aryltetrazolate moiety. Thence, complex $[Ru(4\text{-}TBN)]^{+}$ was treated with 1 equiv of methyl triflate, leading to the formation of the dication $[Ru(4\text{-}(Me)\text{-}TBN)]^{2+}$ (Scheme 2), in which the tetrazolate carbon (Ct) ^{13}CNMR resonance is found at 156.4 ppm and falls in the expected chemical shift range (152−157 ppm) for 5-aryltetrazoles having a substituent at the nitrogen adjacent to tetrazole carbon.[32,33]

In perfect agreement with the analogous organometallic compounds,[17] the analysis of the NMR data suggests that the methylation reaction occurs regioselectively at the N-4 nitrogen (see Scheme 2a)—the one which suffers less encumbrance from the metal fragment—causing the out of plane rotation of the aromatic 5-substituent ring. The consequent loss or, at least, strong reduction of interannular conjugation is indicated by the separation between the chemical shifts of the benzonitrile carbons *meta* and *ortho* in the complex $[Ru(4\text{-}(Me)TBN)]^{2+}$ [$\Delta(\delta(C_{meta})-\delta(C_{ortho}))$ = 3.5 ppm; see Table 3 and Scheme 2b, right], which is significantly lower than that displayed by the precursor $[Ru(4\text{-}TBN)]^{+}$ [$\Delta(\delta(C_{meta})-\delta(C_{ortho}))$ = 6.4 ppm; see Scheme 2b, left]. Further support to our hypotheses is given by the crystal structure of the methylated dication $[Ru(4\text{-}(Me)\text{-}TBN)]^{2+}$ (Figure 2 and Table 2), in which the tetrazole and the benzonitrile rings are considerably out of plane [dihedral angle N(6)−C(26)−C(27)−C(32) = 118.9(6)°]. The large variation of this torsion angle is the only major change introduced in the structure of $[Ru(4\text{-}(Me)TBN)]^{+}$ after methylation, compared to the precursor $[Ru(4\text{-}TBN)]^{+}$, all the other bonding parameters being almost identical.

Similarly, the protonation of $[Ru(4\text{-}TBN)]^{+}$ (Scheme 3) affords the dication complex $[Ru(4\text{-}(H)TBN)]^{2+}$ in which the hydrogen substituent is found on the N-4 tetrazolate nitrogen, as clearly indicated by the ^{13}C NMR data [δ(Ct) = 156.4

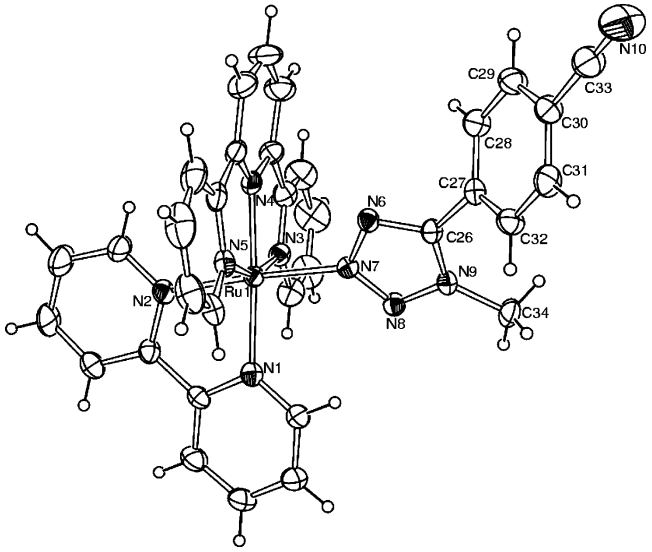

Figure 2. Molecular structure of $[Ru(4\text{-}(Me)TBN)]^{2+}$, with key atoms labeled. Displacement ellipsoids are at 30% probability level.

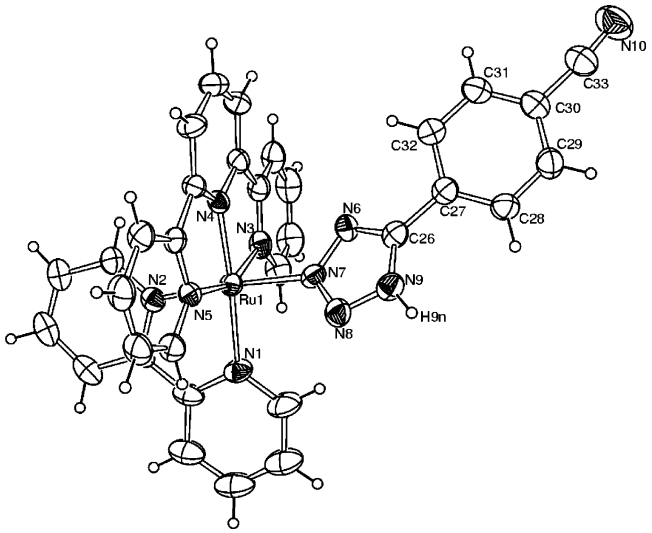

Figure 3. Molecular structure of $[Ru(4\text{-}(H)TBN)]^{2+}$, with key atoms labeled. Displacement ellipsoids are at 30% probability level.

ppm] and the crystal structure of the salt $[Ru(4\text{-}(H)TBN)][CF_3SO_3]_2 \cdot CH_3CN \cdot H_2O$ (Figure 3 and Table 2). Hydrogen bonding is present within the crystal, involving one $CF_3SO_3^-$ anion and the N−H tetrazole group [N(9)···O(6) = 2.774(12) Å, N(9)−H(9n)···O(6) = 159(8)°] and the second $CF_3SO_3^-$ anion and H_2O [O(3)··O(7) = 2.554(12) Å; the water hydrogens have not been located]. As for the methylated analogous $[Ru(4\text{-}(Me)TBN)]^+$, no significant differences in the bond distances and bond angles of $[Ru(4\text{-}(H)TBN)]^{2+}$ compared to $[Ru(4\text{-}TBN)]^+$ are present. It is only important to notice that the dihedral angle between the two aromatic rings of the 5-substituted tetrazole ligand shows an intermediate value [N(6)−C(26)−C(27)−C(32) = 24.6(11)°] between the ones found in $[Ru(4\text{-}TBN)]^+$ [7.3(6)°] and $[Ru(4\text{-}(Me)TBN)]^{2+}$ [118.9(6)°], and this is probably due to the smaller steric hindrance of the hydrogen compared to the methyl group. A similar trend is also observed in the ^{13}C NMR data, where the separation of *meta* and *ortho* carbons for $[Ru(4\text{-}(H)TBN)]^{2+}$ [$\Delta(\delta(C_{meta})-\delta(C_{ortho})) = 5.4$ ppm] is intermediate between the precursor $[Ru(4\text{-}TBN)]^+$ [$\Delta(\delta C_{meta})-\delta(C_{ortho})) = 6.4$ ppm] and the methylated compound $[Ru(4\text{-}(Me)TBN)]^{2+}$ [$\Delta(\delta(C_{meta})-\delta(C_{ortho})) = 3.5$ ppm].

As we might expect,[17] the protonated mononuclear species $[Ru(4\text{-}(H)TBN)]^{2+}$ can be reconverted into the cationic precursor $[Ru(4\text{-}TBN)]^+$ by treatment with a stoichiometric amount of a base such as triethylamine. It is important to point out that the reversibility of the protonation reaction (Scheme 3) offers the opportunity to modulate the structural and electronic properties of the aromatic 5-substituted tetrazolate ligands by a simple protonation−deprotonation mechanism.

Dinuclear Complexes. The ^1H NMR spectrum of the dinuclear complex $[Ru(BTB)Ru]^{2+}$ (Supporting Information, Figure S4a) is found to be closely similar to that of mononuclear compound $[Ru(4\text{-}TBN)]^+$. The presence of the "fully tetrazolate" bridging ligand BTB is demonstrated by the singlet at 7.64 ppm, which is assigned to the four chemically equivalent BTB protons. The ^{13}C NMR spectrum of $[Ru(BTB)Ru]^{2+}$ (Table 3 and Figure S4b) displays a single tetrazole carbon (Ct) resonance at 164.3 ppm, clearly indicating the selective N-2 tetrazole coordination of each of the peripheral Ru(tpy)(bpy) fragment. In the case of the dinuclear species $[Ru(4\text{-}TBN)Ru]^{3+}$, the presence of the nonequivalently bridging ligand [4-TBN$^-$] led to a quite complicated ^1H NMR spectrum in which it was not possible to clearly distinguish the resonance frequencies of protons *ortho* and *meta* (see Figure S5a and Scheme 1 for labeling) from those of the bpy and tpy rings. Concerning ^{13}C NMR spectroscopy, the comparison of the ^{13}C NMR data of the dinuclear complex $[Ru(4\text{-}TBN)Ru]^{3+}$ (Figure S5b) with the ones of the mononuclear building block $[Ru(4\text{-}TBN)]^+$ and of the dinuclear organometallic analogues $[Cp(CO)(L)FeN_4CC_6H_4NFe(L)(CO)Cp]^+$ [17a] allowed the assignment of ^{13}C NMR carbon resonances of the tetrazolate ligand [4-TBN$^-$], which were consistent both with the selective coordination of the Ru(tpy)(bpy) unit to the N-2 tetrazole nitrogen [δ(Ct) = 163.1 ppm] and with the presence of interannular conjugation [$\Delta(\delta(C_{meta})-\delta(C_{ortho})) = 6.4$ ppm] across the bridging linker [4-TBN$^-$].

UV−Vis Absorption and Emission Properties. The electronic spectra of all the complexes, which were measured

Scheme 3. Protonation of $[Ru(4\text{-}TBN)]^+$

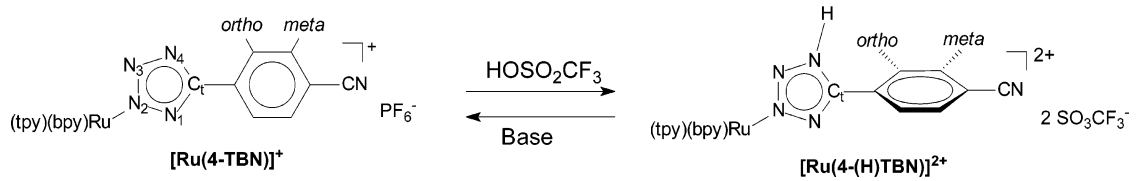

Table 4. Absorption[a] and Emission[a,b] Bands (CH_3CN as Solvent, Room Temperature) of All Complexes

complex	λ/nm ($10^{-4}\epsilon/M^{-1}$ cm^{-1}) LC−MC	MLCT	λ_{em}/nm
$[Ru(tpy)(bpy)Cl]^+$	240 (7.10), 282 (6.62), 294 (7.45), 317 (6.80)	503 (2.21)	nd
$[Ru(4\text{-}TBN)]^+$	248 (6.95), 272 (5.49), 289 (5.90), 313 (6.88)	425 sh (0.97), 482 (1.73)	672
$[Ru(4\text{-}(H)TBN)]^{2+}$	248 (5.61), 272 (5.49), 289 (5.90), 310 (5.26)	459 (1.91)	664
$[Ru(4\text{-}(Me)TBN)]^{2+}$	242 (5.80), 275 (5.24), 291 (5.78), 310 (5.30)	464 (1.37)	616
$[Ru[4\text{-}TBN]Ru]^{3+}$	239 (8.04), 271 (10.4), 287 (11.6), 310 (10.4)	416 sh (2.22), 454 (2.58)	676
$[Ru[BTB]Ru]^{2+}$	232 (7.05), 271 (8.27), 291 (10.5), 312 (10.3)	418 sh (1.03), 480 (2.14)	680

[a] Concentrations: 4×10^{-5} M. [b] Excitation wavelength: 480 nm.

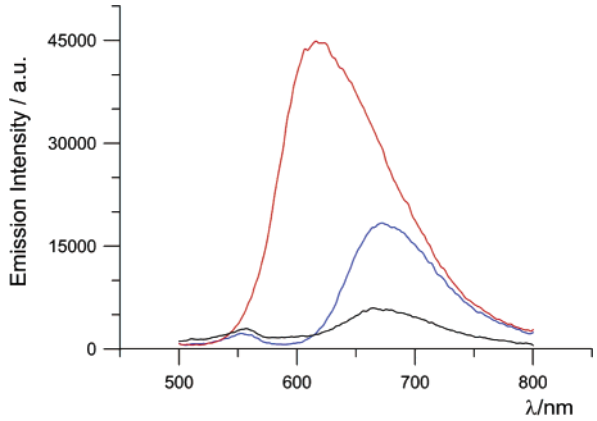

Figure 4. Emission spectra (excitation wavelength, 480 nm; sample concentration, 4×10^{-5} M in acetonitrile) recorded at 25 °C of mononuclear complexes $[Ru(4\text{-}TBN)]^+$ (blue trace), $[Ru(4\text{-}(Me)TBN)]^{2+}$ (red trace), and $[Ru(4\text{-}(H)TBN)]^{2+}$ (black trace).

in acetonitrile solution, are summarized in Table 4. In all cases, the UV region is dominated by intense ligand-centered (LC) $\pi-\pi^*$ transitions, the energies of which are analogous to those of similar Ru(tpy)(bpy)-based complexes.[5a] In addition, as typical for Ru(II)−polypyridyl chromophores, each spectrum displays the metal-to-ligand charge-transfer (MLCT) transitions as the lowest energy (400−600 nm) absorptions. In general, this broadened band is centered between 450 and 480 nm; in some cases (see Table 4) the energy differences between d(Ru)$-\pi^*$(tpy) and d(Ru)$-\pi^*$(bpy) transitions are indicated by the presence of a shoulder in the range 416−425 nm. The increase of the ionic charge on going from complex $[Ru(4\text{-}TBN)]^+$ to the dication complexes $[Ru(4\text{-}(H)TBN)]^{2+}$ and $[Ru(4\text{-}(Me)TBN)]^{2+}$ results in a shift of the maximum of the MLCT bands to higher energy (i.e. $\lambda_{max}^{MLCT} = 464$ nm for $[Ru(4\text{-}(Me)TBN)]^{2+}$ and 459 nm for $[Ru(4\text{-}(H)TBN)]^{2+}$), while marginal changes occurred to the ligand-centered transitions (see Supporting Information, Figure S6).

The emission spectra of all compounds were recorded in acetonitrile at room temperature. Some preliminary studies on the luminescence of all complexes indicated that, by excitation at 480 nm, they show the characteristic emission from ^{3}MLCT excited states. In particular, the luminescence properties of mononuclear complex $[Ru(4\text{-}TBN)]^+$ ($\lambda_{em} =$ 672 nm) can be tuned by addition of electrophiles (Figure 4). Indeed, the protonated compound $[Ru(4\text{-}(H)TBN)]^{2+}$ showed a weaker emission peak at slightly higher energy ($\lambda_{em} = 664$ nm), while a significantly stronger and blue-shifted luminescence is exhibited by the methylated derivative $[Ru(4\text{-}(Me)TBN)]^{2+}$ ($\lambda_{em} = 616$ nm).

This aspect, which is of importance for any future study (as for example, in the bioinorganic chemistry field) of the mononuclear derivative $[Ru(4\text{-}TBN)]^+$, is currently under investigation together with the electrochemical behavior of this species upon addition of electrophiles (vide infra). However, all compounds exhibit a fluorescence efficiency (Φ) in the range between 0.008 (i.e. $[Ru(4\text{-}(Me)TBN)]^{2+}$ and $[Ru(4\text{-}TBN)Ru]^{3+}$) and 0.003 (i.e. $[Ru(4\text{-}TBN)]^+$ and $[Ru(BTB)Ru]^{2+}$). Such values are about 1 order of magnitude lower than that found for $Ru(bpy)_3^{2+}$, which shows a fluorescence efficiency of 0.06 under the same experimental conditions.[1a] Concerning the dinuclear complexes $[Ru(BTB)Ru]^{2+}$ and $[Ru(4\text{-}TBN)Ru]^{3+}$, the relatively good luminescence efficiency and the weak electronic coupling between the metal centers (see spectroelectrochemical results) prompted us to consider these molecules as good candidates for ECL studies.[6a]

Electrochemical Behavior of Ligands and Complexes. Uncoordinated Ligands. It is well established that the redox processes in Ru(II)−polypyridine complexes are mainly localized either on the metal center (oxidations) or on the ligands (reductions).[1,8a,34] It is, therefore, of fundamental importance to know the electrochemical behavior of the uncoordinated ligands to understand the pattern of the ligand-based redox series for the complexes.

The electrochemistry of the uncoordinated ligand bpy[35] has been previously studied under the same experimental conditions used for this work. We investigated the redox behavior of the ligands 4-TBN and BTB, to our knowledge for the first time, either as their tetraphenylarsonium salts or N-protonated species, while tpy was reinvestigated in DMF under strictly aprotic conditions, both at room and low temperature.

4-TBN. The free ligand exists as the N-protonated species 4-TBNH and was investigated in ACN and DMF solutions both in its deprotonated form (i.e. 4-TBN) and as 4-TBNH. In acetonitrile the 4-TBNH shows two one-electron reductions but no oxidation process is observed up to + 2.5 V (vs SCE). Figure 5a shows the CV of 4-TBNH, in DMF at 24 °C and a scan rate, ν, of 1 V/s; the first reduction wave exhibits some degree of electrochemical irreversibility, most likely due to internal rearrangements related to proton

(34) Marcaccio, M.; Paolucci, F.; Paradisi, C.; Roffia, S.; Fontanesi, C.; Yellowlees, L. J.; Serroni, S.; Campagna, S.; Denti, G.; Balzani, V. *J. Am. Chem. Soc.* **1999**, *121*, 10081.
(35) (a) Roffia, S.; Casadei, R.; Paolucci, F.; Paradisi, C.; Bignozzi, C. A.; Scandola, F. *J. Electroanal. Chem.* **1991**, *302*, 157. (b) Roffia, S.; Marcaccio, M.; Paradisi, C.; Paolucci, F.; Balzani, V.; Denti, G.; Serroni, S.; Campagna, S. *Inorg. Chem.* **1993**, *32*, 3003.

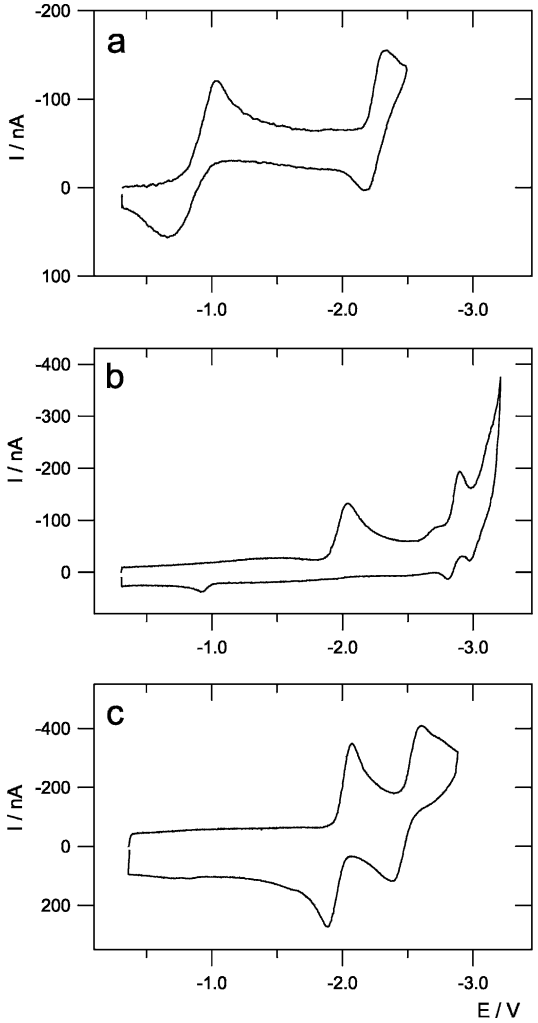

Figure 5. Cyclic voltammetric curves of uncoordinated ligands: (a) 4-TBNH, 1 mM in a 0.05 M TEATFB/DMF solution, working electrode Pt disk, diameter 125 μm, $T = 24$ °C, scan rate 1 V/s; (b) BTB 1 mM in a 0.05 M TEATFB/DMF solution, working electrode Pt disk, diameter 125 μm, $T = 24$ °C, scan rate 10 V/s; (c) tpy 2 mM in a 0.07 M TEATFB/DMF solution, working electrode Pt disk, diameter 125 μm, $T = -56$ °C, scan rate 100 V/s.

Table 5. Half-Wave Potentials $E_{1/2}$ (vs SCE) of the Uncoordinated Ligands and Mono- and Dinuclear Ruthenium Complexes

	oxidn $E_{1/2}$/V		redn $E_{1/2}$/V				
species	1	2	I	II	III	IV	V
tpy[a]			−1.98	−2.50			
4-TBNH[a,b]			−0.87	−2.24			
BTB[a]			−2.03[c]	−2.85	−3.05		
$[Ru(4\text{-}TBN)]^{+}$ [b]	1.02		−1.42	−1.71	−2.19	−2.34	
$[Ru(4\text{-}TBN)Ru]^{3+}$ [b]	1.02	1.32	−1.28	−1.63	−1.96	−2.19	−2.36
			−1.40	−1.70			−2.47
$[Ru(BTB)Ru]^{2+}$ [b]	1.01	1.03	−1.41	−1.71	−2.19	−2.45	
			−1.45	−1.74	−2.24	−2.52	

[a] TEATFB/DMF solution. [b] TBAH/ACN solution. [c] Cathodic peak potential.

migration onto the nitrogens of the tetrazole ring, while the second reduction is Nernstian. The standard potentials of the processes are collected in Table 5, together with those of the other species.

BTB. The $BTBH_2$ ligand has been investigated as the deprotonated species (i.e. the BTB species; see Chart 1) in DMF at room and low temperature. It shows three reductions: the first is completely irreversible even at 200 V/s while the further two processes are reversible. Although the third reduction occurs at the edge of the electrolyte/DMF discharge, it can still be observed as a reversible process. Figure 5b shows the cyclic voltammetric curve of BTB at 24 °C and at 10 V/s. Just before the second voltammetric peak, there is a shoulder whose nature is still under investigation but is probably related to a species generated in a follow-up reaction.

tpy. The voltammetry of uncoordinated terpyridine, previously investigated,[36] shows a one-electron reduction process. It was reinvestigated in DMF, to compare it to the other ligands and complexes under the same strictly aprotic conditions, and it exhibits two reduction peaks both at room and low temperature. The first reduction is a one-electron Nernstian process while the second one-electron reduction shows chemical irreversibility at room temperature but becomes reversible at low temperature and at scan rates higher than 100 V/s.

Figure 5c shows the CV of tpy at −56 °C and 100 V/s. The $E_{1/2}$ values of the two processes are given in Table 5. The separation between them is 520 mV, and this value falls within the typical range (500−600 mV) for the electronic coupling energy[37] into the same orbital of polypyridyl ligands. The chemical follow-up reaction is probably a proton uptake process of the doubly reduced tpy with the solvent. This reaction is a rather fast process even at low temperature, and the voltammetric pattern is similar to other polypyridyl ligands in the uncoordinated state[35,38] that are known to undergo fast protonation reactions in the doubly reduced state.

Ruthenium Mono- and Dinuclear Complexes. $[Ru(4\text{-}TBN)]^{+}$. Within the framework of the general strategy for the investigation of multinuclear species, showing a large number of redox processes, this species was studied since it represents a precursor or a model for the behavior of the dinuclear ones. The electrochemistry of the complex $[Ru(4\text{-}TBN)]^{+}$ was investigated in ACN both at room temperature and at −45 °C. In both cases it shows four one-electron reduction processes and a one-electron oxidation. The first two reductions are completely reversible whereas the successive two are affected by chemical follow-up reactions. With increase of the sweep rate, the extent of the chemical irreversibility decreases, even though it still remains at 100 V/s. As a consequence of the chemical irreversibility of the third process, an anodic peak appears on the reverse scan, at about −1.9 V (Figure 6). The chemical process associated with the third reduction probably involves protonation, either by the solvent or the electrolyte, of one of the tetrazolate nitrogens, whose basicity is increased when the other two ligands are reduced.[39]

(36) Saji, T.; Aoyagui, S. *J. Electroanal. Chem.* **1975**, *58*, 401.
(37) Marcaccio, M.; Paolucci, F.; Paradisi, C.; Carano, M.; Roffia, S.; Fontanesi, C.; Yellowlees, L. J.; Serroni, S.; Campagna, S.; Balzani, V. *J. Electroanal. Chem.* **2002**, *532*, 99 and references therein.
(38) Krejčik, M.; Vlček, A. A. *J. Electroanal. Chem.* **1991**, *313*, 243.
(39) Further investigations concerning the nature and the mechanism of such reaction are currently being undertaken.

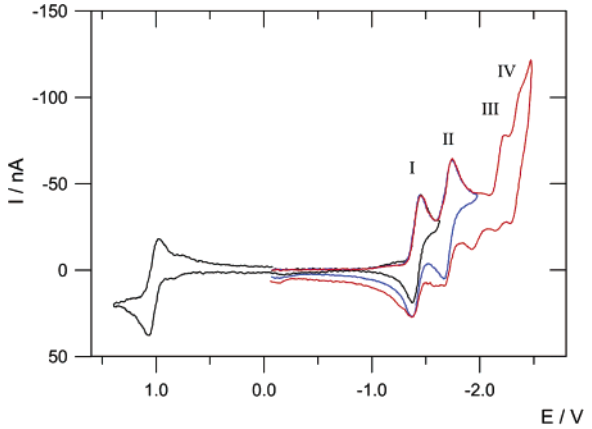

Figure 6. Cyclic voltammetric curve for 1 mM mononuclear complex $[Ru(4\text{-}TBN)]^{+}$ in a 0.06 M TBAH/ACN solution: working electrode Pt disk; diameter 125 μm; $T = 25$ °C; scan rate = 1 V/s.

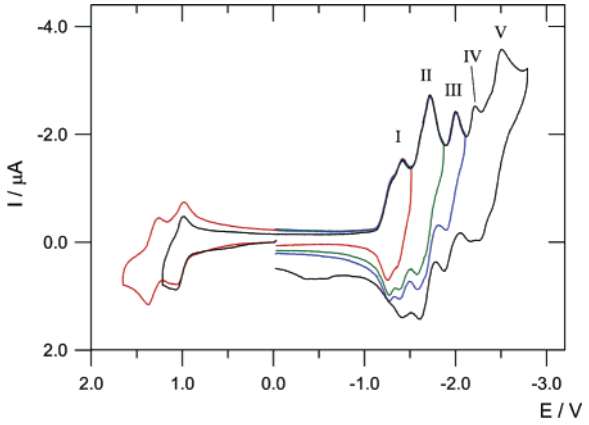

Figure 7. Cyclic voltammetric curve of 1 mM of dinuclear complex $[Ru(4\text{-}TBN)Ru]^{3+}$ in 0.05 M TBAH/ACN solution: working electrode Pt disk; diameter 125 mm; $T = 25$ °C; scan rate = 1 V/s.

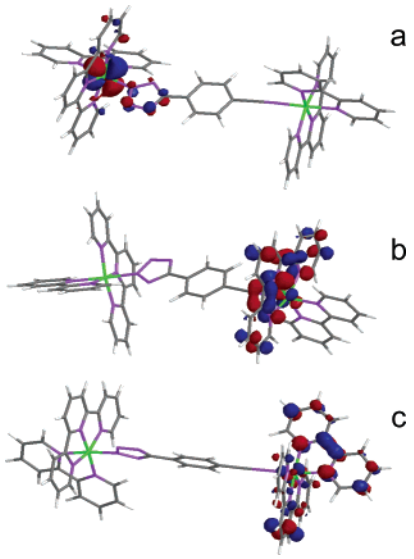

Figure 8. Molecular orbital surfaces of $[Ru(4\text{-}TBN)Ru]^{3+}$ showing the localization of relevant orbitals involved in the redox processes: (a) HOMO (first oxidation) mainly centered on the ruthenium coordinated to tetrazolate; (b) LUMO (first reduction) centered on the tpy; (c) third unoccupied MO (third reduction process) centered on bpy ligand.

The oxidation process appears chemically and electrochemically reversible at 1 V/s. As the scan rate is increased, the process reveals some degree of electrochemical irreversibility. The simulation of the cyclic voltammetric curve, comprising the oxidation and the first reduction wave, confirms that the oxidation is not a fully Nernstian process. A satisfactory agreement of the simulated curve with the experimental one is obtained when the heterogeneous constant k_h for the oxidation process is 4×10^{-2} cm/s and the electron-transfer coefficient α of the Butler−Volmer equation is 0.34. By contrast, the reduction process is satisfactorily simulated as a fast (diffusion-controlled) electron transfer. This can be understood on the basis of quantum molecular orbital calculations, carried out at DFT level (see Supporting Information), where it is shown that the HOMO spans over the metal centers and part of the bridging ligand, in particular on the tetrazolate ring (see the corresponding dinuclear species, Figure 8a). The sluggishness of the electron transfer is therefore most probably associated with molecular rearrangement of the tetrazolate ligand, following the oxidation process. However, the reductions are centered onto the polypyridine ligands (vide infra), as also evidenced by the calculations, and these are intrinsically fast processes.

$[Ru(4\text{-}TBN)Ru]^{3+}$. On the basis of the behavior of the mononuclear species, which is one of the two constituent moieties of the complex $[Ru(4\text{-}TBN)Ru]^{3+}$, it is possible to rationalize the electrochemistry of the dinuclear species, whose cyclic voltammetric curve is shown in Figure 7.

The bridging ligand can be considered as electronically asymmetric because the two coordinating nitrogens are chemically different: one belongs to the tetrazolyl ring and bears a partial negative charge while the other can be considered to be a nitrile-N for its coordinating properties.

The voltammetric curve shows five reduction peaks and two oxidation ones. Concerning the oxidations, the two peaks are both reversible one-electron processes, centered on the two Ru(II) centers. The sizable separation between the oxidations suggests a quite strong metal−metal bridge-mediated interaction, but it could also be ascribed to the electronically asymmetric coordinating ends of the bridging ligands, giving rise to two nonequivalent ruthenium centers with different oxidation potentials. Probably this potential separation arises from an interplay of these two effects, with the second more important. A comparison of the $E_{1/2}$ potentials of the first oxidation of this dinuclear complex with that of the oxidation of the mononuclear precursor species $[Ru(4\text{-}TBN)]^{+}$ shows that the processes happen at the same value. Therefore the first oxidation of the dinuclear is centered on the ruthenium bound to tetrazolate moiety of the bridging ligand. A DFT calculation also supports this assignment of the oxidation processes to the HOMO mainly centered onto the ruthenium coordinated to tetrazole (Figure 8a) and the second highest occupied MO onto the second metal center, coordinated to the nitrile end of the bridge.

$[Ru(BTB)Ru]^{2+}$. The voltammetric behavior of the dinuclear complex carrying the symmetric BTB bridging ligand is shown in Figure 9, and it consists of five voltammetric peaks: one in the oxidation region and the remaining in reduction. All the peaks are two-electron processes, as evidenced by chronoamperometric measurements. The elec-

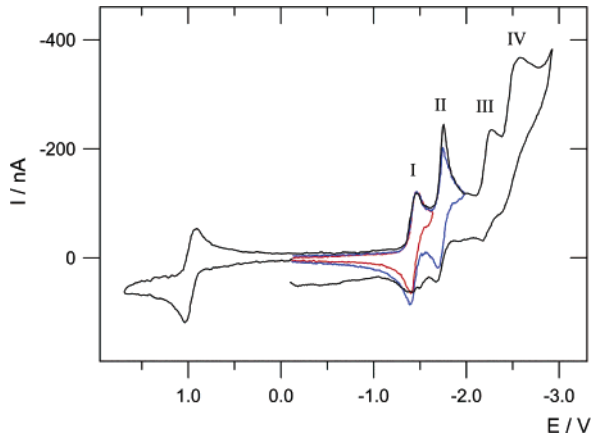

Figure 9. Cyclic voltammetric curve of 1 mM of dinuclear complex [Ru(BTB)Ru]$^{2+}$ in 0.05 M TBAH/ACN solution: working electrode Pt; T = 25 °C; scan rate = 1 V/s.

trochemical behavior is very similar to that of the mononuclear [Ru(4TBN)]$^{+}$ species which is, in fact, the building block of the dinuclear complex [Ru(BTB)Ru]$^{2+}$. The cyclic voltammetric curve shown in Figure 9 suggests that the first two reduction peaks are strongly affected by adsorption or precipitation phenomena. Moreover, the processes in the last two peaks are partially affected by chemical follow-up reactions.

The electron-transfer processes in each of the voltammetric peaks are very close each other, and the evaluation of the $E_{1/2}$ values was carried out by digital simulation of the voltammetric curves. Accordingly, the two processes comprised in each peak have a separation in the range 30−60 mV (see Table 5), which is slightly larger than the separation due to the statistical factor for systems with very weakly interacting redox centers.[40] Thus, there is little delocalization across the BTB bridge, suggesting the same holds true for the 4-TBN-bridged species, as also indicated by DFT calculations and spectroelectrochemical results.

To understand the main localization of the reduction processes for the mono- and dinuclear complexes, the behavior of the uncoordinated ligands must be taken into account, together with a comparison of the $E_{1/2}$ values of the corresponding processes for related complexes and results of the quantum molecular calculations. The reduction processes of the mononuclear species [Ru(4-TBN)]$^{+}$ can be assigned as follows: The first is attributed to tpy, since it is slightly easier to reduce than bpy, and hence, the subsequent reduction is centered onto bpy. The third process might be reasonably assigned to 4-TBN, and the last represents the second reduction (electron pairing into the same redox orbital) of the tpy. However, if the voltammetric curve (see also the $E_{1/2}$ values in Table 5) of the mononuclear is compared with those of the dinuclear species [Ru(4-TBN)Ru]$^{3+}$ and [Ru(BTB)Ru]$^{2+}$, the last two processes of the mononuclear should be assigned to the second reduction onto tpy and bpy, respectively. Such an attribution is also supported by the separation between the first and the second set of peaks (i.e. between the second and third one), which reflects the energy of electron pairing into polypyridyl ligands. Thus the reduction centered onto 4-TBN is not observed since it is outside the negative limit of the useful potential window. On the basis of the assignments of reductions for [Ru(4-TBN)]$^{+}$, we can obtain those for [Ru(4-TBN)Ru]$^{3+}$. The processes within the first two peaks are localized onto the two tpy's and the two bpy's. As expected, molecular orbital calculations indicated that the first reduction is localized on the tpy bound to ruthenium coordinated to the nitrile end of the 4-TBN bridging ligand (Figure 8b). Again, the first bpy to undergo reduction (i.e. the third one) is that coordinated to the ruthenium−nitrile moiety, as shown in Figure 8c by the prevalent localization of the third unoccupied MO. The fifth reduction (i.e. the third peak) has a potential which does not match any process in the corresponding mononuclear species, and then it can be confidently attributed to the bridging ligand 4-TBN. The coordination to two metal centers shifts the unobservable process in the mononuclear to one occurring at less negative potentials, falling within the useful potential window. The process in the fourth peaks and the two in the fifth peak can be attributed as the second reduction of three out of four polypyridyl ligands (tpy and bpy), on the basis of the comparison of the $E_{1/2}$ values in Table 5.

Finally, the localization of the reductions for the [Ru(BTB)Ru]$^{2+}$ is quite straightforward comparing the CV curves and the potentials of processes. The first pair of two-electron peaks represents the first reduction of the two tpy's and two bpy ligands. The last two peaks (four electrons) are the electron couplings onto the same redox orbital centered on each polypyridine.

UV−Vis−NIR Spectroelectrochemistry of Dinuclear Complexes. The UV−vis−NIR spectroelectrochemical investigation of the two dinuclear complexes was carried out at room and low temperature (−32 °C) in ACN and DMF for the oxidation and the reduction processes respectively, under strictly aprotic conditions as for the voltammetric study. The investigation only of the oxidation processes will be discussed, since it is related to the evaluation of the intramolecular metal−metal communication. The reductions are mainly centered on the ligands, and the results merely confirmed the assignments of the various processes previously made on the basis of electronic and electrochemical arguments.

[Ru(4-TBN)Ru]$^{3+}$. The UV−vis−NIR spectrum of the complex [Ru(4-TBN)Ru]$^{3+}$ shows two main regions: the MLCT transitions in the visible, centered at about 23 000 cm^{-1}, and the rather intense $\pi-\pi^*$ intraligand absorptions in the UV. As discussed above, the species undergoes two well-separated one-electron oxidations, and upon performing the first oxidation process, we observe spectral changes consisting of a decrease in the intensity of MLCT bands and at the same time the appearance of new transitions in the NIR and UV regions together with a modification of those attributed to $\pi-\pi^*$ intraligand transitions. As shown in Figure 10a, the band in the NIR around 12 000 cm^{-1} is rather broad and weak. This is clearer in the inset of Figure 10a,

(40) Flanagan, J. B.; Margel, S.; Bard, A. J.; Anson, F. C. *J. Am. Chem. Soc.* **1978**, *100*, 4248.

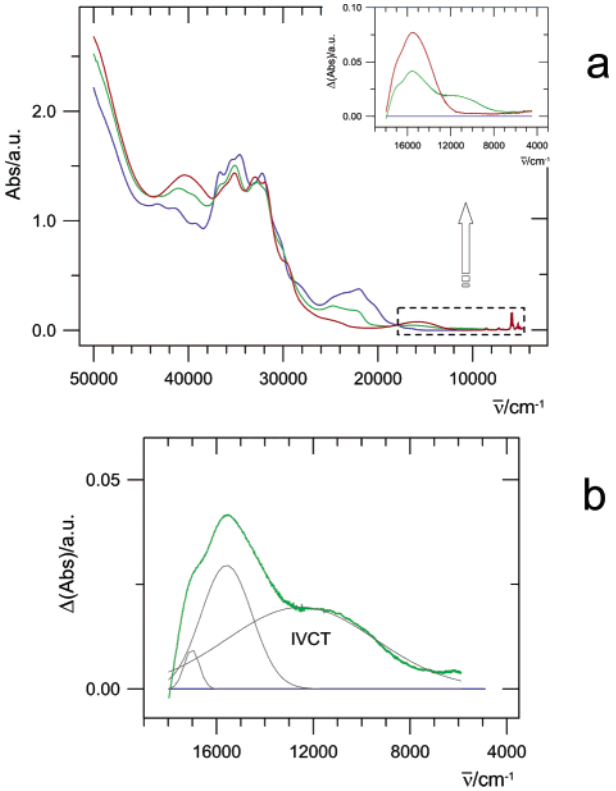

Figure 10. UV−vis−NIR spectroelectrochemistry of a 0.6 mM [Ru(4-TBN)Ru]$^{3+}$ in 0.08 M TBAH/ACN solution: (a) spectra of the pristine compound (blue trace), one-electron-oxidized species (green trace), and doubly oxidized complex (red trace) with inset showing the difference spectra (spectrum of the pristine complex subtracted) in the NIR region of the one- and two-electron-oxidized species; (b) Gaussian deconvolution of the difference spectrum of one-electron-oxidized product as in the inset of (a).

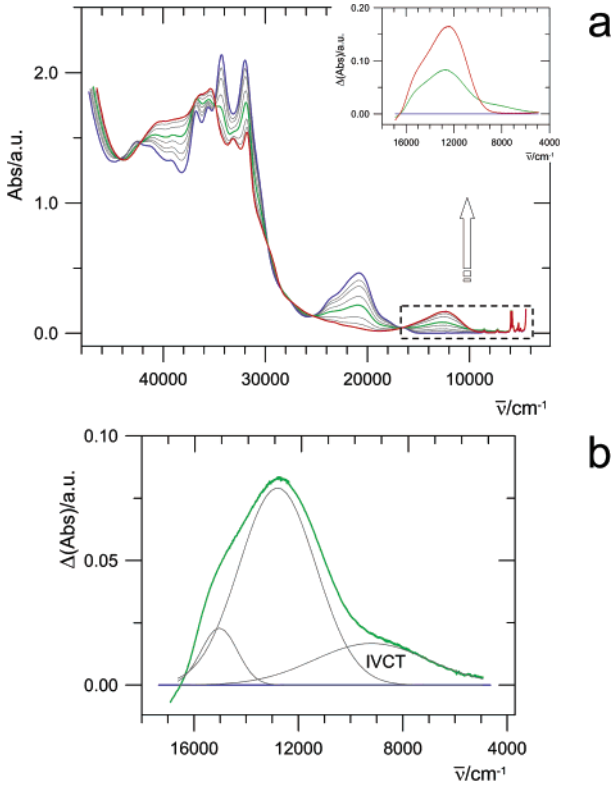

Figure 11. UV−vis−NIR spectroelectrochemistry of a 0.6 mM [Ru(BTB)-Ru]$^{2+}$ in 0.08 M TBAH/ACN solution: (a) spectra of the pristine compound (blue trace), one-electron-oxidized species (green trace), and doubly oxidized species (red trace) with inset showing the difference spectra in the NIR region of the one- and two-electron-oxidized species (with same colors); (b) Gaussian deconvolution of the difference spectrum of one-electron-oxidized product as in the inset of (a).

where the difference spectra of the singly and doubly oxidized species are shown. Upon the second oxidation, the MLCT band disappears completely, the spectral evolution in the UV region continues, and, most importantly, the weak and broad NIR band collapses. This is a clear indication that this band is an intervalence charge transfer band (IVCT), only observed in the mixed-valence species, which grows with the oxidation of one of the two metal centers and disappears completely upon the removal of the second electron from the dinuclear species. In Figure 10b the difference spectrum of the first oxidation product (green trace) has been deconvoluted into three Gaussian components of which the broadest one centered at $\lambda = 800$ nm (12 550 cm^{-1}), which disappears upon the second oxidation, is the IVCT band.

[Ru(BTB)Ru]$^{2+}$. The spectroelectrochemistry of the dinuclear complex [Ru(BTB)Ru]$^{2+}$ is shown in Figure 11, and the behavior is very close to that described above for the other dinuclear species. During the two one-electron oxidation processes the MLCT absorptions gradually decrease and eventually disappear. The $\pi-\pi^*$ intraligand bands move to higher energy, and some transitions develop in the NIR region (Figure 11a). Although the two oxidation processes for this complex are very close to each other, careful control of the oxidation potential during the spectroelectrochemical investigation allowed us to obtain the mixed-valence species.

Again, the Gaussian deconvolution of the difference spectrum for the first oxidation product (Figure 11b) gives three components, only one of which (9200 cm^{-1}, i.e., $\lambda = 1090$ nm) is rather broad and disappears upon the subsequent oxidation, while the other two increase. This is a clear indication that this weak band is an IVCT band. The intensities of the deconvoluted IVCT bands of the dinuclear complexes [Ru(4-TBN)Ru]$^{3+}$ and [Ru(BTB)Ru]$^{2+}$ are 1090 M^{-1} and 935 M^{-1} cm^{-1}, respectively. According to the Hush model[7c,41] the magnitude of the metal−metal coupling energies is 500 and 313 cm^{-1}, respectively. The separation between the metal centers, for the estimation of electronic coupling, was obtained from the optimized molecular structures of the species at the DFT level. The energy values so obtained can be considered as a lower limit, since the redox centers involved are not strongly localized on the metal atoms but partially involve the tetrazole rings of the bridging ligands, as shown by molecular orbital results above; therefore, the appropriate dipole distance in calculating the IVCT oscillator strength is shorter, which results in larger electronic metal−metal coupling.[41]

Electrogenerated Chemiluminescence. The ECL spectra of [Ru(BTB)Ru]$^{2+}$ and [Ru(4-TBN)Ru]$^{3+}$ obtained by alternating generation of the one electron oxidized and reduced

(41) Crutchley, R. J. *Adv. Inorg. Chem.* **1994**, *41*, 273 and references therein.

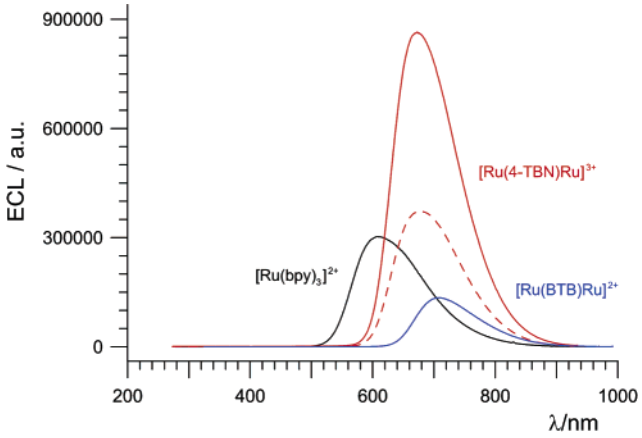

Figure 12. ECL spectra of the reference compound $[Ru(bpy)_3]^{2+}$ (black trace), $[Ru(BTB)Ru]^{2+}$ (blue trace), and $[Ru(4\text{-}TBN)Ru]^{2+}$ (red traces). The dashed red line for $[Ru(4\text{-}TBN)Ru]^{2+}$ is the spectrum obtained by annihilation of one-electron-oxidized and -reduced forms; the full red line is obtained for the doubly oxidized and reduced forms of complex. All ECL spectra were collected for 1 mM ACN solutions and TBAH as supporting electrolyte, 25 °C, and accumulation time 4 min.

forms in ACN containing 0.1 M of TBAH as supporting electrolyte are shown in Figure 12. Emission was not seen by eye indicating that either the ECL yield is not very high or it falls in the red region. However, the results were completely reproducible over a wide number of experiments performed with the same solution. This would indicate that the systems studied are quite stable and therefore promising for future use in devices. On the basis of the absorption and emission wavelengths of the compound, the energy needed to generate the first singlet-excited state is about 1.77 eV for $[Ru(BTB)Ru]^{2+}$ and 1.86 eV for $[Ru(4\text{-}TBN)Ru]^{3+}$. These energy values are therefore those that must be generated in the electrochemical annihilation reaction of the oxidized and reduced species (radical ions) to generate the excited state and ECL emission. In a typical ECL experiment, the radical anion reacts with the radical cation; however, in our case, it was also possible to study the effect of the generation of doubly reduced and doubly oxidized species for $[Ru(BTB)Ru]^{2+}$ and $[Ru(4\text{-}TBN)Ru]^{3+}$. The best result for compound $[Ru(BTB)Ru]^{2+}$, in terms of ECL intensity, was obtained when the potential was stepped between 1.4 and −1.6 V (vs silver wire quasi reference electrode). In this potential range the first two-electron reduction and the first two-electron oxidation were included. No difference in the ECL signal was observed when extending the potential window further while a lower intensity was obtained for 1.1/−1.8 and 1.1/−1.6 potential ranges, with the last interval leading to the smallest signal of all. Compound $[Ru(4\text{-}TBN)Ru]^{3+}$ showed very interesting results both considering the one-electron oxidation/reduction and the doubly oxidized/reduced forms. The ECL spectra of $[Ru(BTB)Ru]^{2+}$ and $[Ru(4\text{-}TBN)Ru]^{3+}$ are characterized by broad emission bands between 640 and 850 nm and between 600 and 860 nm, respectively. The maxima for both compounds were at 710 nm for $[Ru(BTB)Ru]^{2+}$ and 680 nm for $[Ru(4\text{-}TBN)Ru]^{3+}$. When compared to the fluorescence, the ECL spectra show some differences, being slightly broader in shape with the λ_{max} at about the same value or eventually shifted to lower energy (about 30 nm for $[Ru(BTB)Ru]^{2+}$). This difference is probably due to the lower resolution in the ECL instrument where the spectra were collected. In addition, the observed ECL emission band shows significant emission in the longer wavelength region as compared to the fluorescence spectrum. Such a lower energy emission, as previously observed for other systems,[42] might be due to the formation of side products generated during the annihilation. At the same time the fact that no change in the absorption and fluorescence spectra was observed before and after extensive potential cycling demonstrates that this is not the case. The longer wavelength component in the ECL could also be due to the formation of excited-state aggregates at the concentration used to obtain the spectrum, although this also appears unlikely. ECL yields were determined against a standard (the ECL system containing 1 mM of $[Ru(bpy)_3]^{2+}$ in 0.1 M TBAH/ACN with $\phi_{ECL} \cong 0.05$)[43] by comparison of the measured integrated photon intensities, taking into account the differences in the electric charges passed through the solution studied.

The ECL efficiencies of $[Ru(BTB)Ru]^{2+}$ and $[Ru(4\text{-}TBN)Ru]^{3+}$ are about 40% and 150% of that of $Ru(bpy)_3^{2+}$, respectively. The 4-TBN dinuclear complex shows an efficiency much higher than that of related ruthenium complexes containing tpy as ligand, which are known to have a low luminescence efficiency at room temperature.[1c,8c,d]

The ECL efficiency (in photons emitted/electron transferred between reduced and oxidized forms of the parent molecule) is related directly to the yield of the excited state on annihilation (ϕ_{es}) and to the emission quantum yield (ϕ_o) of a given emitter ($\phi_{ecl} = \phi_{es}\phi_o$). The result implies that the yield for the formation of the excited states is close to 100%. This is promising for future development of these systems. The enthalpy for the annihilation reaction is sufficient to generate the emitting state. For the process $\Delta H^\circ_{ann} = \Delta G^\circ_{ann} + T\Delta S^\circ$, this value is based on the half-wave potentials of the first oxidation and reduction wave in the cyclic voltammogram ($\Delta E_{1/2}^{(ox/red)} \approx 2.5$ V for both compounds), and if we consider an entropy effect ≅ 0.1 eV, we obtain a value of 2.4 eV which is in both cases (compound $[Ru(BTB)Ru]^{2+}$ and $[Ru(4\text{-}TBN)Ru]^{3+}$) is higher than the minimum energy required for the population of the excited state from which the emission takes place.

Conclusions

Tetrazole-based compounds are a kind of a "missing link in the family tree" represented by five-membered N-heterocyclic compounds commonly incorporated in polypyridine complexes of Ru(II). The introduction of 5-aryltetrazolate ligands leads to a class of complexes that are interesting from different viewpoints. First, the planar arrangement which is adopted by the tetrazolate ligand 4-TBN in the corresponding mononuclear complex $[Ru(4\text{-}TBN)]^+$ might indeed represent a promising feature for the

(42) Lai, Y. R.; Kong, X.; Jenekhe. S. A.; Bard, A. J. *J. Am. Chem. Soc.* **2003**, *125*, 12631.
(43) Rubinstein, L.; Bard, A. J. *J. Am. Chem. Soc.* **1981**, *103*, 6641.

use of this compound as a metallointercalator for DNA or related nucleotides. Note that the geometry of the ligand, as well as its electronic properties, can be modified either permanently or in a reversible way. Furthermore, NMR evidence indicates that the main structural and electronic features of the 5-aryl-substituted ligands are also maintained in the corresponding dinuclear complex $[Ru(4\text{-}TBN)Ru]^{3+}$. The spectral, photophysical, and redox properties of the complexes have been investigated. In the electrochemistry of those species, the reduction processes are mainly centered on the ligands and the sites of the various processes have been identified on the basis of the behavior of the uncoordinated ligands and a comparison between the species herein studied. The oxidations are mainly metal-centered, and the electrochemical and UV−vis−NIR spectroelectrochemical data indicate that these tetrazolate bridging ligands mediate the electronic interactions between the two ruthenium centers. Finally, the photophysical properties and especially the very efficient ECL of the complexes investigated are very encouraging for a future development of these species in electrochemiluminescent devices.

Acknowledgment. We thank Dr. Simone Zanarini for helping us with some ECL measurements. We also thank Professor Alberto Arcioni for helpful discussions. The financial support from MIUR (PRIN 2004035330 and PRIN—"New strategies for the control of reactions: interactions of molecular fragments with metallic sites in unconventional species"), University of Bologna, the National Science Foundation (Grants CHE 0304925 and 0202136), and BioVeris Corp. is gratefully acknowledged.

Supporting Information Available: An experimental section, reporting NMR data and spectra, UV−vis absorption spectra of mononuclear complexes, and computational details, and X-ray crystallographic files in CIF format for the structure determinations of complexes $[Ru(4\text{-}TBN)]^{+}$, $[Ru(4\text{-}(Me)TBN)]^{2+}$, and $[Ru(4\text{-}(H)\text{-}TBN)]^{2+}$. This material is available free of charge via the Internet at http://pubs.acs.org.

IC0514905